

HANOI NATIONAL UNIVERSITY OF EDUCATION
FACULTY OF PHYSICS

LE THI HUONG

**GALAXY COLLISIONS
AS POSSIBLE SOURCES OF
ULTRAHIGH ENERGY
COSMIC RAYS**

DIPLOMA IN ASTROPHYSICS
SPECIALITY: COSMIC RAY PHYSICS

Supervisor: Prof. Pierre DARRIULAT

HANOI, MAY 2008

CONTENT

Acknowledgements

Preamble

1. Cosmic rays

1.1 A brief history

1.2 General features

1.3 Atmospheric showers and the Pierre Auger Observatory

1.4 The sources

1.5 Acceleration in shocks

 First order Fermi acceleration

 Interstellar medium and magnetic fields

 Supernova remnants

 Shock dynamics

 Energy spectrum

 Magnetic field amplification and turbulences

1.6 Cosmic rays: a summary

2. Galaxy collisions

2.1 Generalities on galaxies

2.2 Galaxy collisions: an introduction

2.3 Active galactic nuclei (AGN): an introduction

2.4 Centaurus A: presentation

2.5 Centaurus A: two galaxies

2.6 Centaurus A: the central AGN

2.7 Centaurus A: other features

Summary and perspectives

Bibliography

Acknowledgements

This work was made during a stay at the Vietnam Auger Training Laboratory (VATLY), a cosmic ray laboratory installed at Hanoi in the premises of the Institute for Nuclear Sciences and Technology (INST) which depends from the Vietnam Atomic Energy Commission (VAEC). I am grateful to the members of the Laboratory for having guided me throughout this work and for having given me much useful advice.

I should like to express my heartfelt and deep gratitude to Prof Pierre Darriulat who guided me with enthusiasm throughout the time I spent on this dissertation.

I also thank my teachers at the Department of General Physics of Hanoi University of Education, and particularly Pr Phung Van Dong and Dr Nguyen Quynh Lan.

I would like to thank the young members of the VATLY team: Pham Thi Tuyet Nhung, Pham Ngoc Dong, Nguyen Thi Thao and Pham Ngoc Diep for their help during the time I worked there

I thank my family and my friends who always have been ready to help me with the completion of this work.

The time I spent in VATLY was very short but was an invaluable experience not only in learning physics but also in learning the style of team work, the method of scientific research and how to work efficiently.

Preamble

Recent years have witnessed spectacular progress in our understanding of cosmic ray physics: their sources and the mechanism of acceleration are no longer as mysterious as they were a few years ago; this progress is a direct consequence of important advances in observational astrophysics, including gamma ray astronomy and cosmic ray detection. Three components have been identified: solar cosmic rays at low energies, galactic cosmic rays at intermediate energies and extragalactic cosmic rays at extreme energies. In all three cases diffusive shock acceleration, implying a universal power law energy spectrum, stands out as a privileged candidate for the acceleration mechanism. Most of the evidence comes from detailed studies of the galactic component which has been shown to have its source in the shock region of young supernova remnants. This, together with other considerations including the recent evidence obtained by the Pierre Auger Observatory (PAO) for a strong correlation between ultra high energy cosmic rays (UHECR) and active galactic nuclei (AGN) rich regions, points to large extragalactic shocks being the sites of UHECR acceleration. Among these, colliding galaxies and merging galaxy clusters, which are rich in AGNs, are popular candidates. The present work is made of two parts. A first part reviews the evidence for diffusive shock acceleration after a brief summary of the essential features and properties of cosmic rays. The second part reviews current knowledge of colliding galaxies with particular emphasis on Centaurus A, a nearby active elliptical galaxy which has recently merged with a smaller spiral and is known to be a source of UHECRs from the PAO observations.

1. Cosmic rays

1.1 A brief history

At the end of the XIX^e century, scientists were puzzled by the spontaneous discharge of their electroscopes which suggested the presence of an ionizing radiation. In 1909, Wulf noted that the rate of discharge was decreasing with altitude (Eiffel tower). Between 1911 and 1913 the Austrian physicist Viktor Hess established the existence of an unknown penetrating radiation, coming from above and most probably of extraterrestrial origin, with balloon measurements reaching up to five kilometers in altitude (Figure 1). He shared the 1936 Nobel Prize with Carl Anderson.

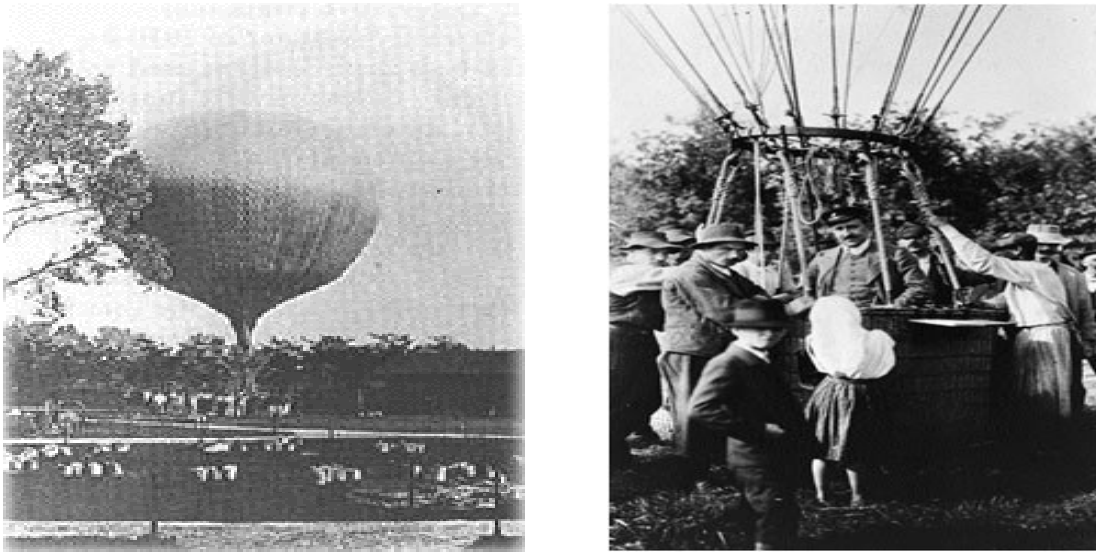


Figure 1 Viktor Hess preparing for a balloon expedition.



Figure 2: Millikan at Pikes Peak.

unambiguously that cosmic rays were charged particles, not photons. In 1938, Pierre Auger (Figure 3), using counters in coincidence, discovered extensive air showers and understood that they were produced by very high energy (up to 10^{15} eV) primaries interacting with the Earth atmosphere.

In the thirties and forties, when accelerators were not yet dominating the scene, cosmic rays became the laboratory for the study of particle physics. Anderson (Figures 4 and 5) discovered the positron in 1932 and the muon in 1938. Powell and Occhialini discovered the pion in 1947. Then

In the following years cosmic rays became the subject of intense research, in particular with Millikan (who coined the name in 1925) and Anderson at Pikes Peak (Figure 2).

In 1927 the dependence on latitude and east-west asymmetry established

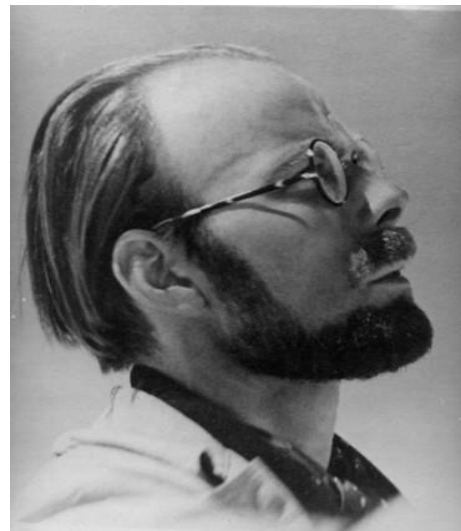


Figure 3: Pierre Auger at the Jungfrau Joch

came strange particles, kaons, hyperons and many others. In the fifties, accelerators took over and cosmic rays got studied for their own sake.



Figure 4: Anderson at Caltech with his cloud chamber.

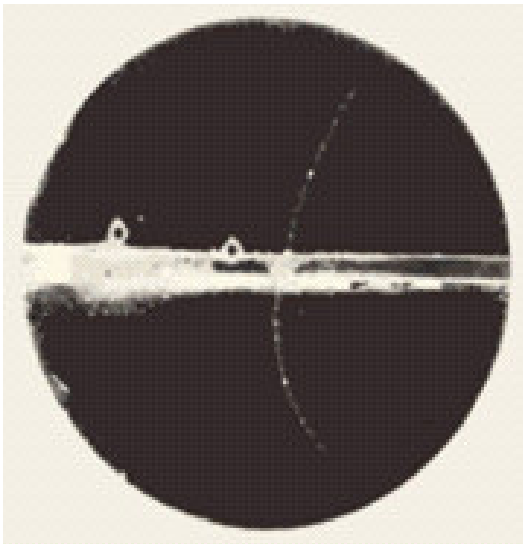


Figure 5: A typical positron event. The positron is flying downwards and loses energy while crossing the lead plate in the middle: Hence a smaller radius of the trajectory (the magnetic field is normal to the figure). This excludes the possibility of an electron flying upwards.



Figure 6: John Linsley at Volcano Ranch chasing a rattle snake out of a hay stack protecting some equipment.

For many years following, major effort was devoted to the study of cosmic rays, trying to understand their origin. Ground detectors, large arrays and fluorescence telescopes, reached very high energies. John Linsley (Figure 6) at Volcano Ranch detected the first 10^{20} eV shower in 1962.

Space astronomy has been a break through for the study of low energy cosmic rays, in particular solar energetic particles (SEP). A recent example of space measurements in solar astronomy is NASA's Advanced Composition Explorer ACE (Figure 7) which was launched from Cape Canaveral in 1997 to the Lagrange point between Sun and Earth.

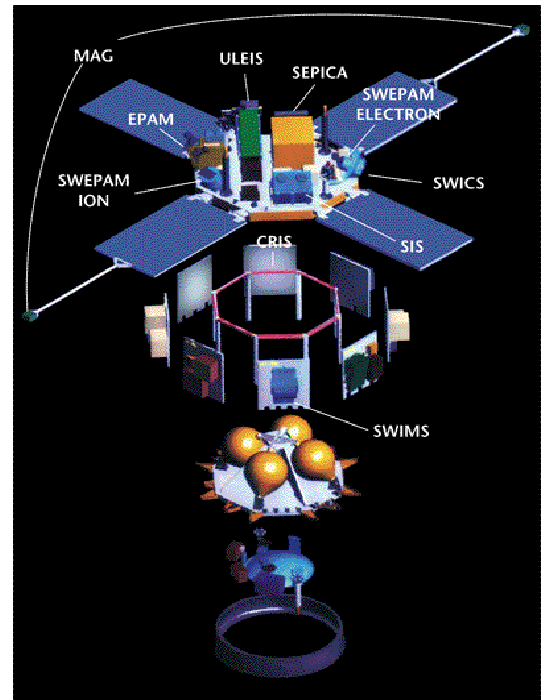


Figure 7: ACE

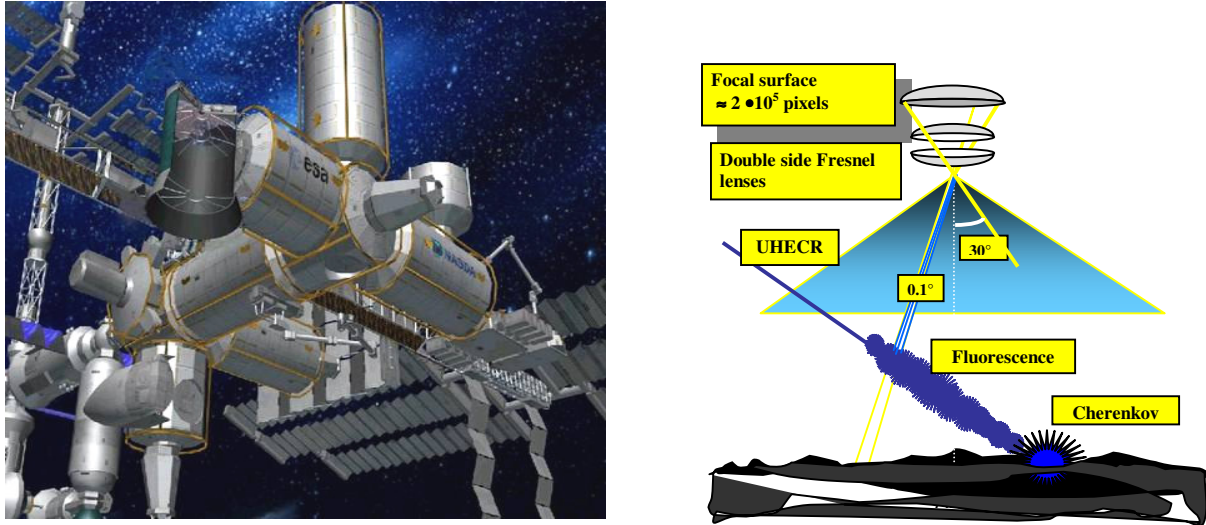


Figure 8: EUSO in the space station (left) and schematic principle (right).

In the past 20 years, spectacular progress in astrophysics, and long time scales implied in the construction of very high energy accelerators, have caused a burst of interest in cosmic ray physics under the name of astroparticle physics. In particular TeV gamma ray detectors have been constructed and operated. Their main asset is that they can point to the sources without suffering deflections from magnetic fields. To study cosmic rays, a new generation of ground detectors was born. In particular, the Pierre Auger Observatory is a huge and hybrid detector covering 1500 km^2 ; showers are detected from the fluorescence they produce in atmosphere and by their impact on a ground detector array. Plans to use the whole Earth atmosphere as a radiator observed from space (Figure 8) are being implemented. Neutrino astronomy is currently being pioneered.

1.2 General features

Cosmic rays are known to be fully ionized atoms, namely atomic nuclei. Their elemental abundance follows closely that in the Universe (Figure 9) with hydrogen and helium being essentially primordial and dominant.

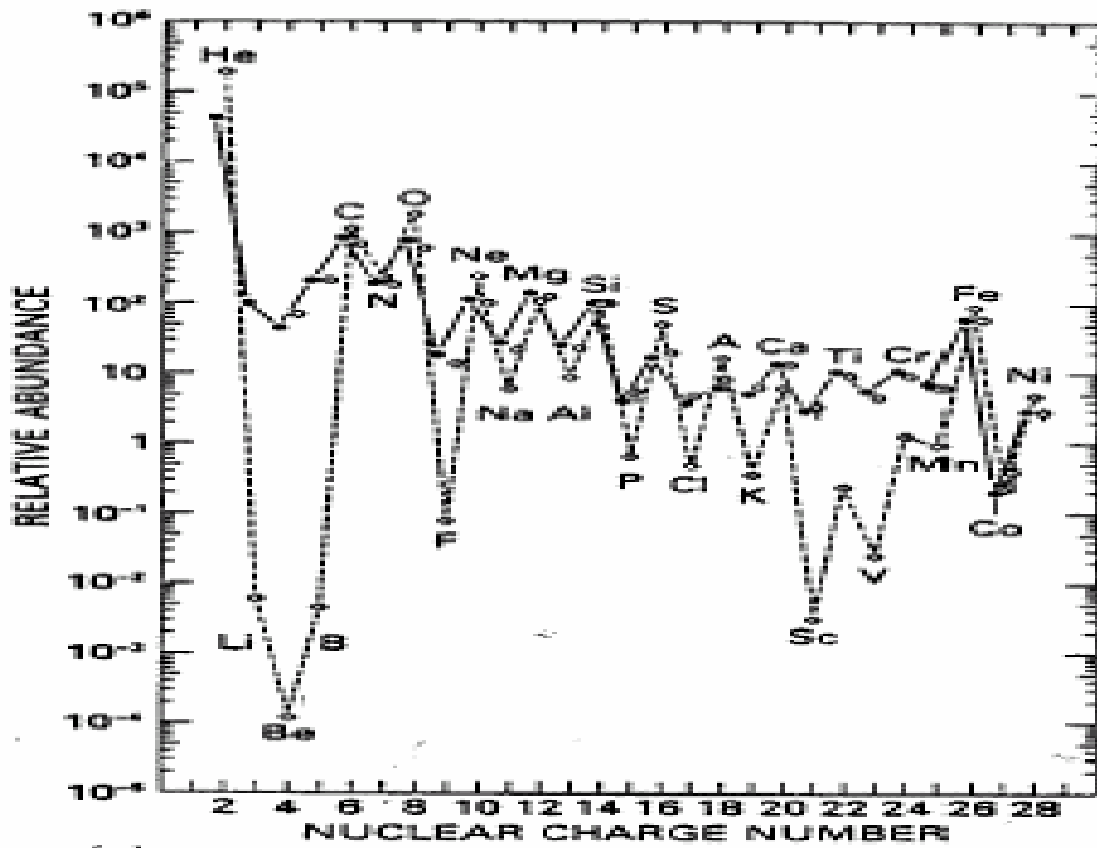


Figure 9: Elemental abundances of cosmic rays (full lines) and of interstellar matter (dotted lines).

Heavier elements have been produced in stars and supernova explosions. Even-even nuclei, which can be considered as made of alpha particles loosely bound to each other, are naturally favoured and the iron region which corresponds to the strongest nuclear binding is enhanced.

Whenever they have been measured, cosmic ray abundances are similar to elemental abundances observed in their environment, suggesting that they have been accelerated from interstellar matter (Figure 9). The main difference is that the valleys are filled by spallation reactions on matter in the interstellar medium ($\sim 7 \text{ gcm}^{-2}$).

Cosmic rays travel in space up to extremely high energies, $\sim 10^{20} \text{ eV} = 16 \text{ Joules}$! There are very few of them but they carry as much energy as the CMB or the visible light or the magnetic fields, $\sim 1 \text{ eV/cm}^3$. They have a power law spectrum covering 32 decades (12 decades in energy), $\sim E^{-2.7}$. Their energy density is $\sim 10^{-12} \text{ erg/cm}^3$.

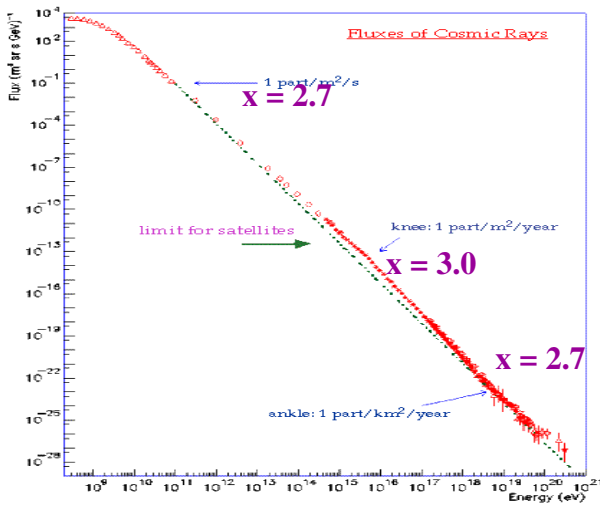


Figure 10: Energy dependence of the cosmic ray flux.

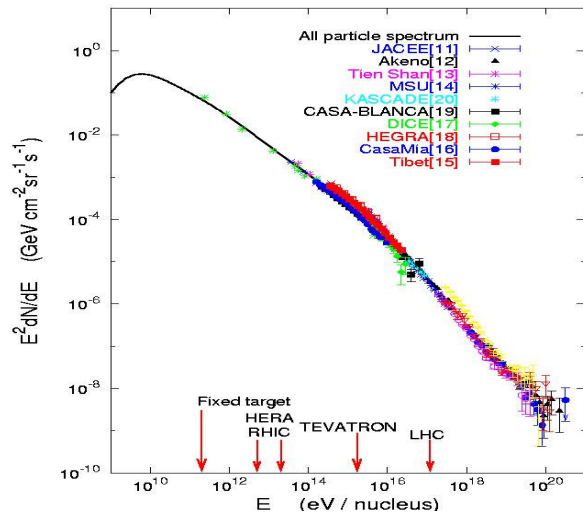


Figure 11: Energy dependence of the high energy flux multiplied by the cube of the energy.

While very low energy cosmic rays are of solar origin, they cannot reach the Earth because they are shielded by the Earth magnetic field. Most higher energy cosmic rays come from our galaxy, the Milky Way, and are trapped in the magnetic field ($\sim 3 \mu\text{G}$) of its disk for some $3 \cdot 10^6 \text{ y}$ (corresponding to the 7 gcm^{-2} quoted earlier). At the lower energy end, the

Earth magnetic field prevents cosmic rays to reach the Earth: in Hanoi this so-called rigidity cut-off amounts to 17GeV.

As we shall see below, supernovae are believed to be the sources of these galactic cosmic rays. It is therefore interesting to compare the power stored in cosmic rays with that released in supernovae explosions: the cosmic ray power amounts to $\sim 10^{-26}$ erg/cm³s; that of SN explosions is 10^{51} erg/SN times some 3 SN per century in the disk, namely some 10^{-25} erg/cm³s. This is about one order of magnitude higher than the power contained in cosmic rays, implying a $\sim 10\%$ efficiency in the energy conversion process.

The highest energy cosmic rays are very rare and are of extragalactic origin. One calls them ultra high energy cosmic rays (UHECR). Their energy density can be estimated to be of the order of $2 \cdot 10^{-19}$ erg/cm³. This implies a power (over an estimated time of 10^{10} y) of some $1.3 \cdot 10^{37}$ erg/Mpc³/s to be compared with powers available from active galactic nuclei (AGN), 10^{44} erg/s/AGN. Another interesting comparison is with gamma ray bursts (GRB): for some 1000 GRB per year, one would need to use an energy of a few 10^{52} erg/GRB.

While the differential spectral index is nearly constant over the whole energy range, a change is seen to occur at $\sim 3 \cdot 10^{15}$ eV where it increases from 2.7 to 3.0. This is called the “knee” (Figure 11). The steeper slope continues to $3 \cdot 10^{18}$ eV where the earlier value of 2.7 is restored: this is called the “ankle”. These fine structures are not very well understood but can be accounted for under reasonable hypotheses (Figure 12).

An important feature of the cosmic ray spectrum is associated with interactions with the CMB causing a ultra high energy cut-off referred to

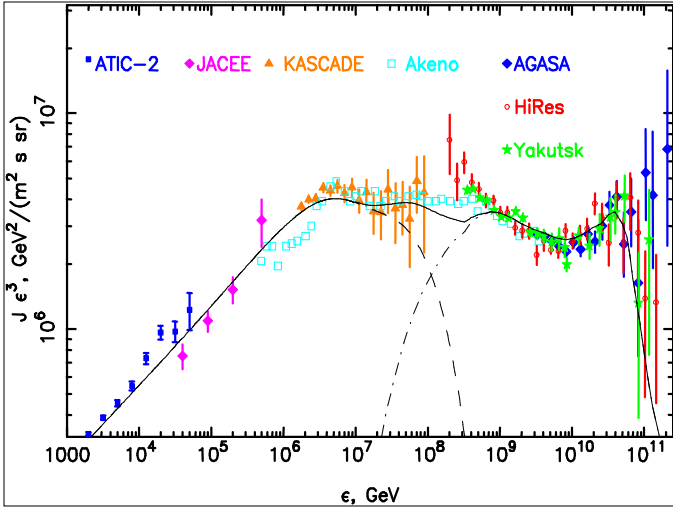


Figure 12: Cosmic ray flux multiplied by the cube of the energy and compared with model predictions.

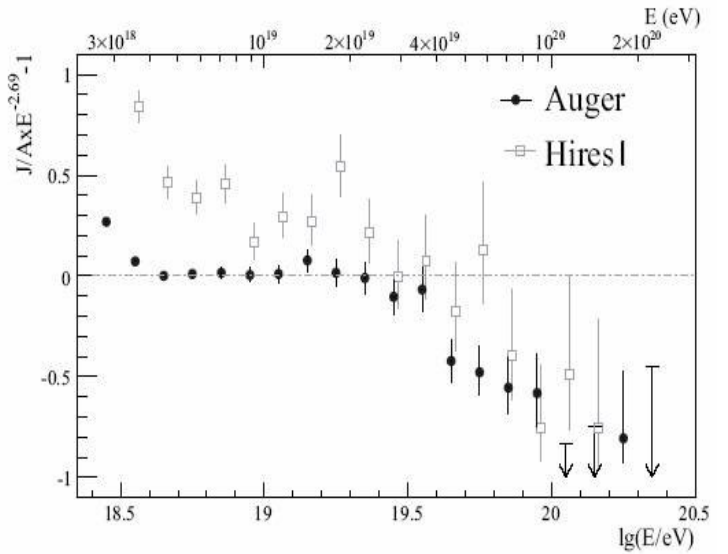


Figure 13: The GZK cutoff as evidenced by the PAO.

as the Greisen Zatsepin Kuzmin (GZK) cut-off (Figures 13 and 14). Photoproduction of pions is expected to occur above a threshold of some 10^{20} eV.



Figure 14: Zatsepin laying down cables.

interacting, and therefore losing energy: their flux will be significantly damped (Figure 15). Only nearby (<100 Mpc) sources can contribute to the UHECR spectrum. While earlier results were inconclusive,

$$\begin{aligned}
 & \text{Indeed for } p + \gamma \rightarrow p + \pi \\
 & M^2(p+\pi) = M_p^2 + 2(E_p + P_p)E_\gamma \approx \\
 & M_p^2 + 2 M_p M_\pi ; M_p M_\pi \approx 2E_p E_\gamma \\
 & \text{As } E_\gamma = 2.7K = 3 \cdot 10^{-4} \text{ eV}, \\
 & E_p = \frac{1}{2} 0.14 \cdot 10^{18} \cdot 10^4 / 3 = 2 \cdot 10^{20} \text{ eV}.
 \end{aligned}$$

With a typical interaction length in the few 10 Mpc scale, cosmic rays coming from larger distances will not make it to the Earth without

the Auger data have now sufficient statistics to establish unambiguously the existence of the GZK threshold.

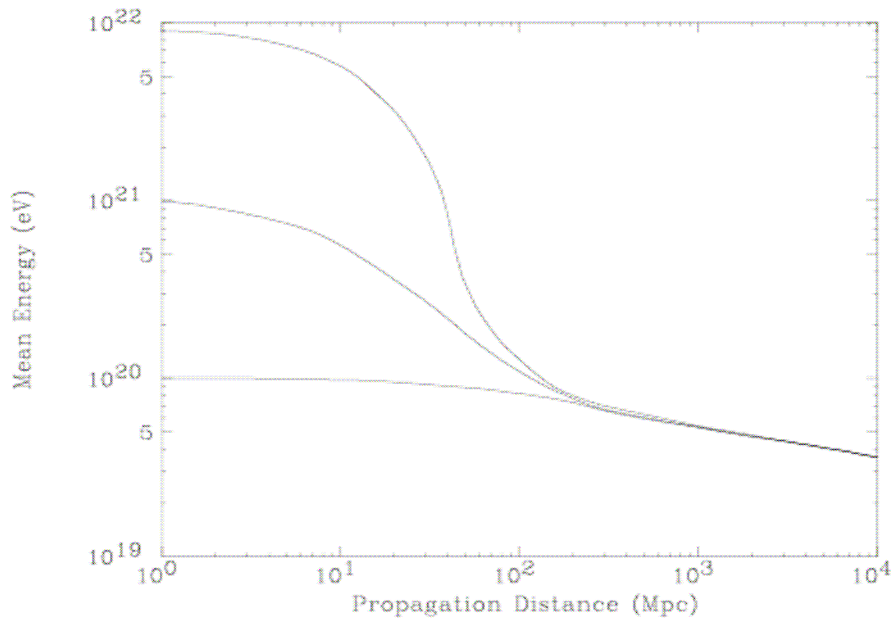


Figure 15: The effect of the GZK cutoff on cosmic rays having original energies of 10^{22} , 10^{21} and 10^{20} eV respectively.

1.3 Atmospheric showers and the Pierre Auger Observatory.

On ground, cosmic rays are detected from their interaction with the air atmosphere. This results in what is called “extensive air showers”. In the present section we say a few words about the way they develop and are detected. We use as an example the case of the Pierre Auger Observatory (PAO) with which VATLY is associated.

Showers have two components, an electromagnetic component and a hadronic component. They are formed by a chain of interactions with a characteristic scale defined by the radiation length in the electromagnetic case and by the interaction length in the hadronic case. As these scales are an order of magnitude shorter than the atmosphere thickness, many successive interactions take place with an accordingly exponential increase of the multiplicity of secondaries. At the same time, secondaries loose energy by

ionization and eventually stop. As a result the shower multiplicity goes through a maximum and then decreases (Figure 16). Electromagnetic showers contain electrons, positrons and photons. The basic interactions are pair creation, $\gamma \rightarrow e^+e^-$ and bremsstrahlung, $e^\pm \rightarrow e^\pm\gamma$. These showers are

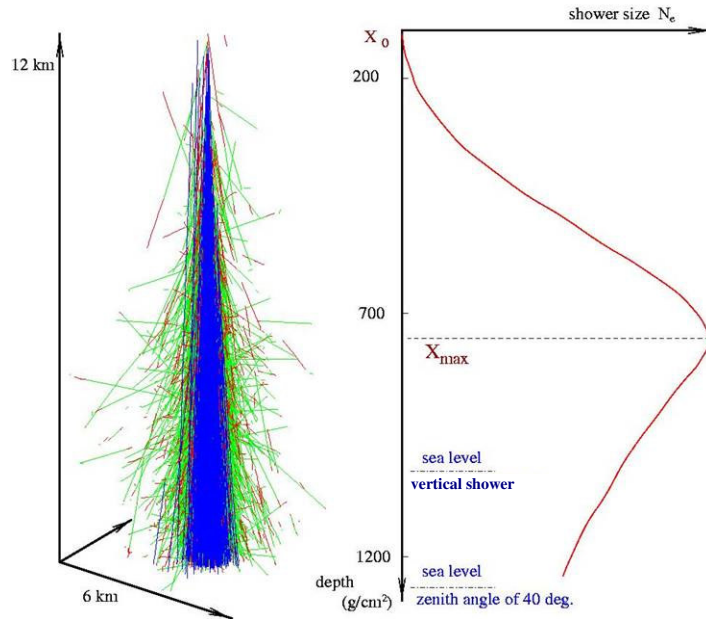


Figure 16: Longitudinal development of an extensive air shower.

initiated by photons from the decay of neutral pions produced in the hadronic interactions. As these decays are instantaneous, neutral pions decay before having a chance to interact with the atmosphere. On the contrary, charged pions have a small decay probability and will interact again with the atmosphere, generating the development of hadronic showers. There the basic interaction is between an atmospheric nucleus and a hadron (nucleon or pion) from the shower, each producing a high multiplicity of new pions.

The air thickness at which the shower reaches its maximum, X_{\max} , is the sum of the thickness where the primary cosmic ray had its first interaction, X_0 and the thickness taken by the shower to reach its maximum, $X_{\max}-X_0$, a quantity which depends only, on average, on the shower energy. The value of X_0 depends on the nature of the primary (proton or heavier nucleus) and the measurement of X_{\max} is therefore important in this context (Figure 17).

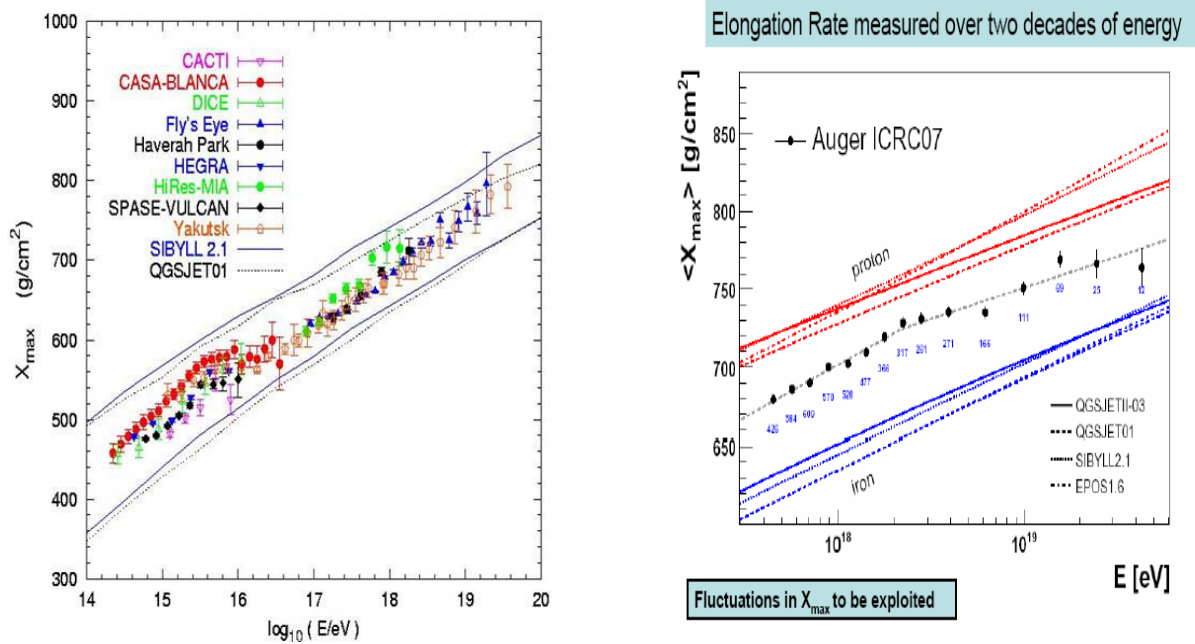


Figure 17: Energy dependence of X_{\max} over the whole range (left) and in the UHECR region (right).

A direct measurement of the shower energy is obtained by detecting the fluorescence induced on nitrogen in the atmosphere (near UV), which measures the longitudinal shower profile. A less direct but easier measurement can be made on ground by sampling the particle density (Figure 18) using an array of counters.

The simultaneous use of both methods is very benefic as it allows for a cross calibration (Figure 19) and because the systematic uncertainties which affect the two methods are very different.

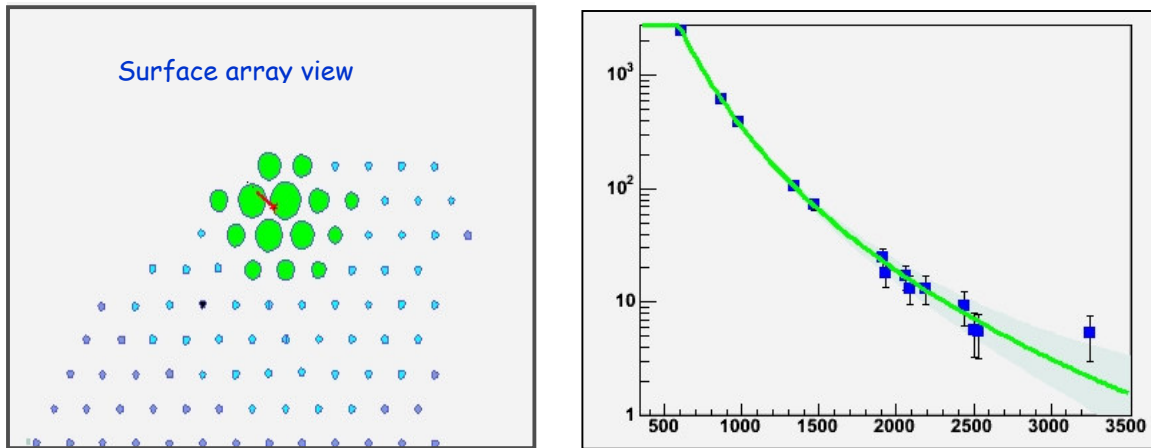


Figure 18: Energy measurement on ground: the signal intensities detected in each tank (left) are plotted as a function of their distance to the barycentre (right). The normalization to a standard reference curve measures the energy.

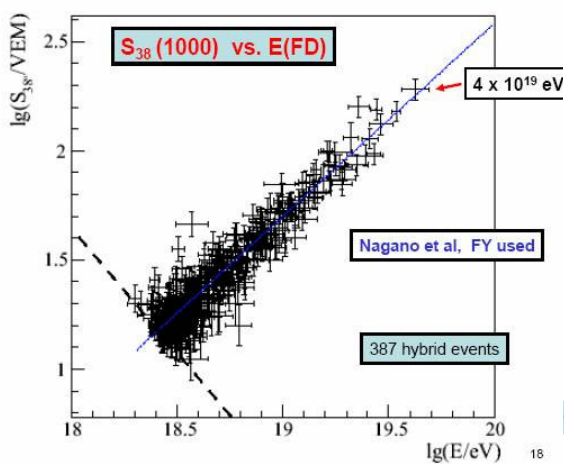


Figure 19: Cross-calibration using hybrid events (abscissa=fluorescence, ordinate=ground).

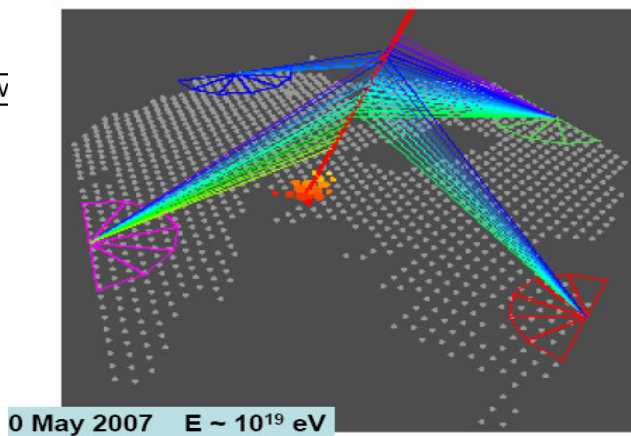


Figure 20: The first PAO hybrid event.

One then talks of hybrid detectors, which is the case of the PAO (Figure 20).

The ground array of the PAO (Figure 21) includes 1600 Cherenkov counters (Figure 22) covering an area of 3000 km^2 while its fluorescence detector (Figure 23) counts 4×6 telescopes which can be operated on clear moonless nights, implying a 10% duty cycle. In both cases timing gives the direction (to within 1°) and intensity gives the energy (to within 10%). Data are transferred by radio to an acquisition centre which filters them and sends them to the laboratories associated with this research.

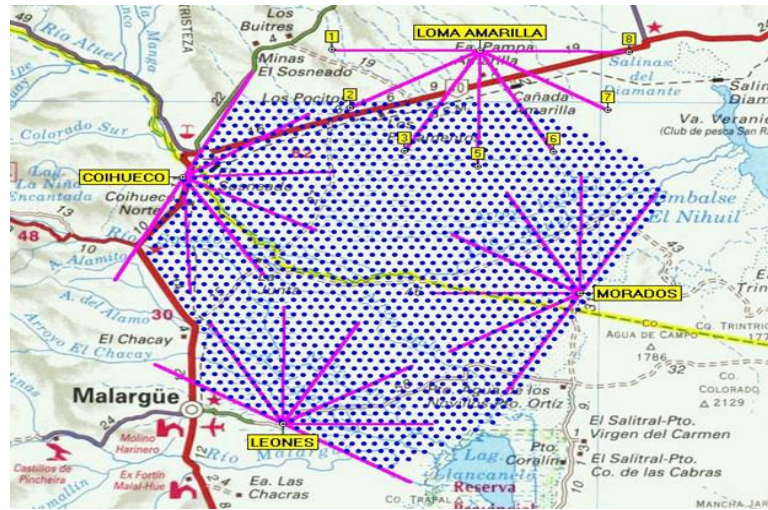


Figure 21: The PAO ground array showing Cherenkov counters (blue dots) and fluorescence eyes (purple lines).

While the ground array is not yet fully completed, the Observatory already reported two important results: it has given evidence for the interaction of UHECRs with the CMB (GZK cut-off described earlier) and it has shown that at least part, if not all, UHECRs originate in regions which are rich in AGNs.

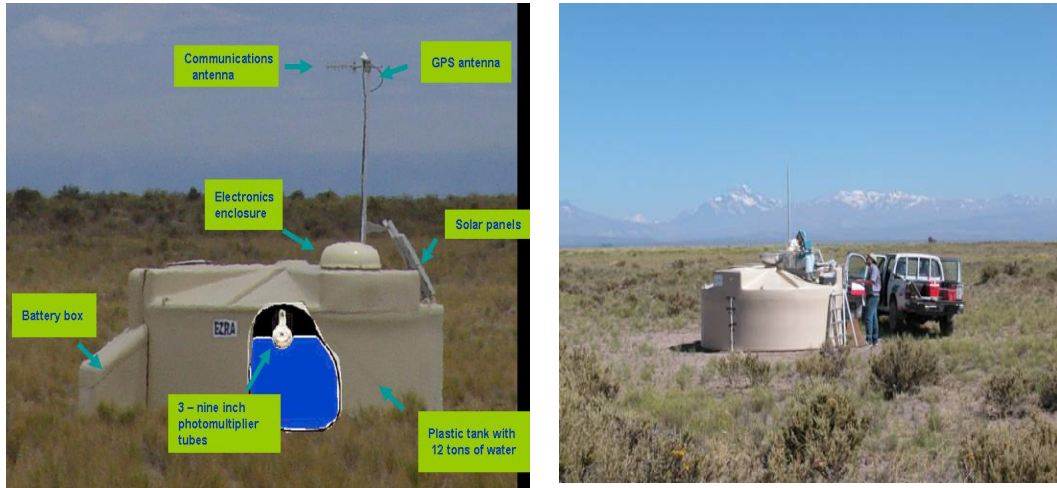


Figure 22: The Cherenkov counter of the PAO ground array.

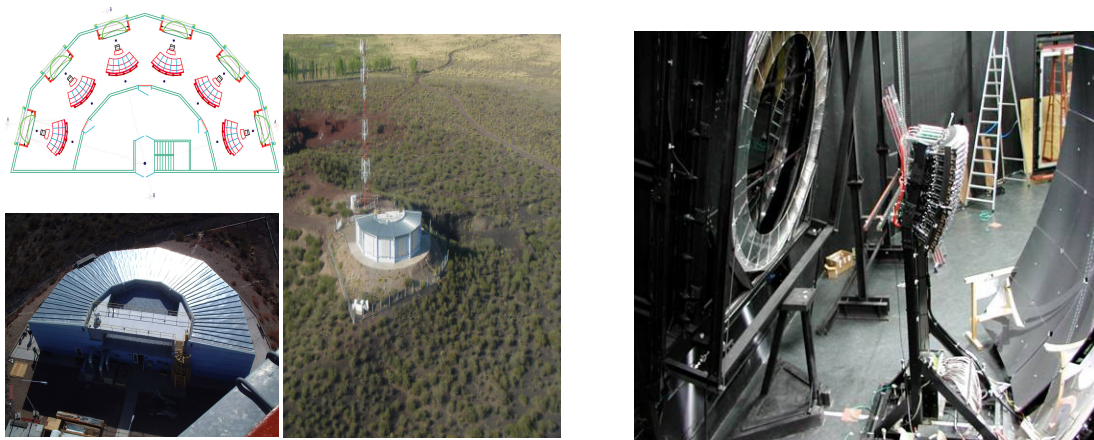


Figure 23: The fluorescence eyes of the PAO; overall view of a station (left) and details of the eye instrumentation (right).

1.4 The sources

Particles coming from the Sun have typical energies in the keV range and make the solar wind (Figure 24). They are mostly associated with solar activity and flares (magnetic field lines recombination and field inversion

with a 11 y cycle). Coronal Mass Ejections (CME) and interplanetary shocks (most of these caused by CME) are similarly correlated (Figure 25).

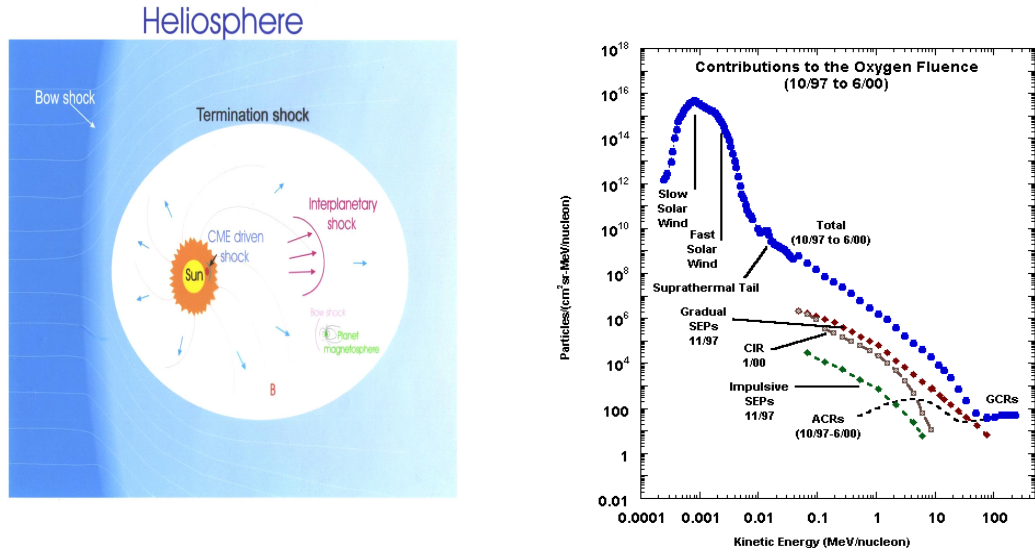
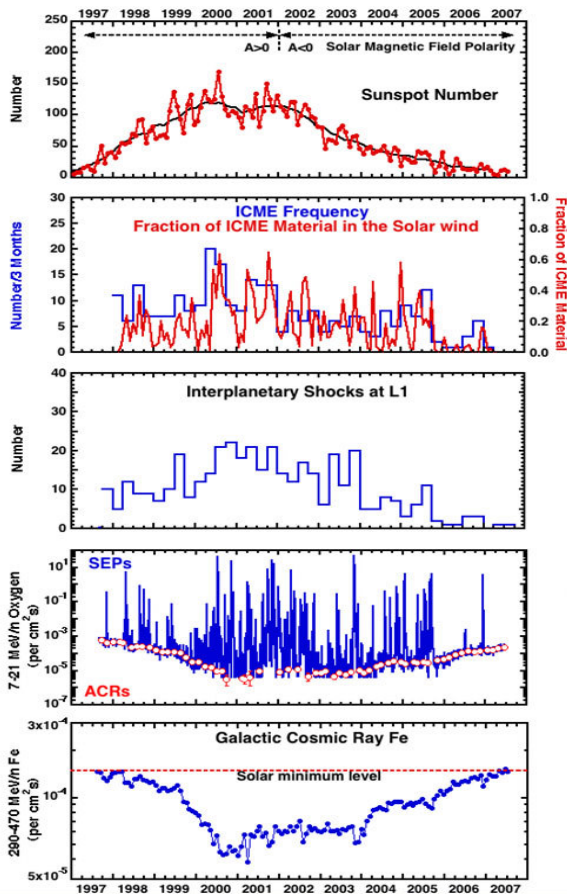


Figure 24: Solar energetic particles, heliosphere (left) and energy dependence of the flux (right).



On the contrary, galactic cosmic rays are anticorrelated with the solar activity which increases the magnetic field and its shielding effect. Solar cosmic rays accelerated on shocks resulting from the solar activity are much rarer and can reach up to 100 MeV.

As previously mentioned, most

Figure 25: Dependence on calendar year of (from top to bottom): Number of sun spots, ICME frequency, interplanetary shocks at L1, SEPs and ACRs, galactic cosmic rays.

cosmic rays are of galactic origin and are accelerated in supernova remnants. It is gamma ray astronomy which has given evidence for this. As gamma rays are photons and therefore are not bent by magnetic fields, they point to their sources (Figure 26).

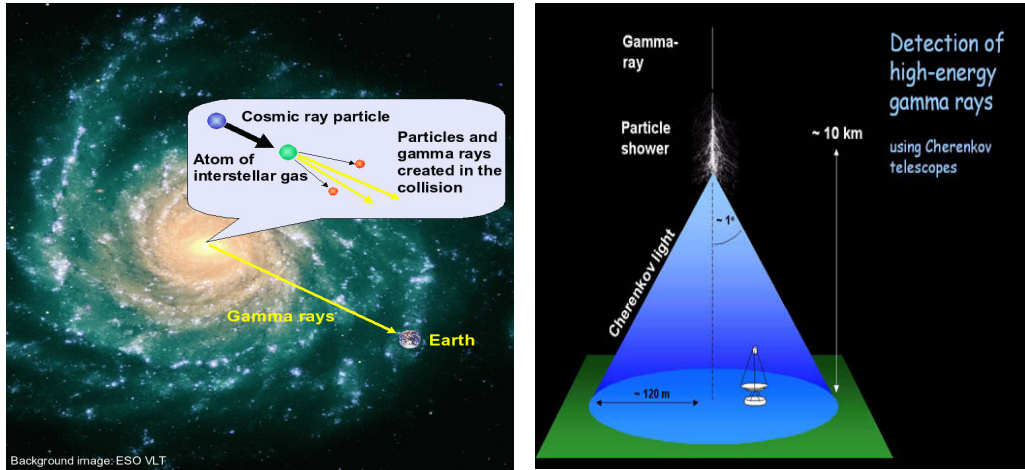
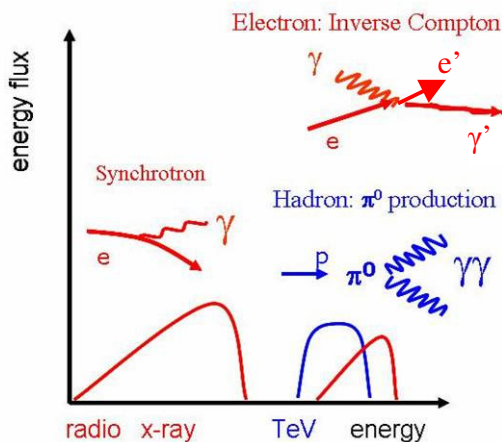


Figure 26: Gamma ray astronomy, main features.

Such high energy gamma rays can originate from cosmic rays interacting with their environment near their sources and producing high energy neutral pions which decay immediately in two gamma rays. In such cases gamma rays act as tracers of cosmic ray sources.



Another source of high energy gamma rays is the interaction of high energy electrons with the CMB photons (Figure 27), a process referred to as inverse Compton (IC).

Figure 27: Components of non thermal gamma rays.



Figure 28: HESS.

The High Energy Stereoscopic System (HESS, Namibia) is made of four telescopes at the corners of a $120 \times 120 \text{ m}^2$ square, operating above 100 GeV (Figure 28). Its field of view is 5° and its resolution a few arc minutes. A picture of the Crab takes only 30 seconds. HESS has established that most galactic cosmic rays originate from Supernova remnants (SNRs) by

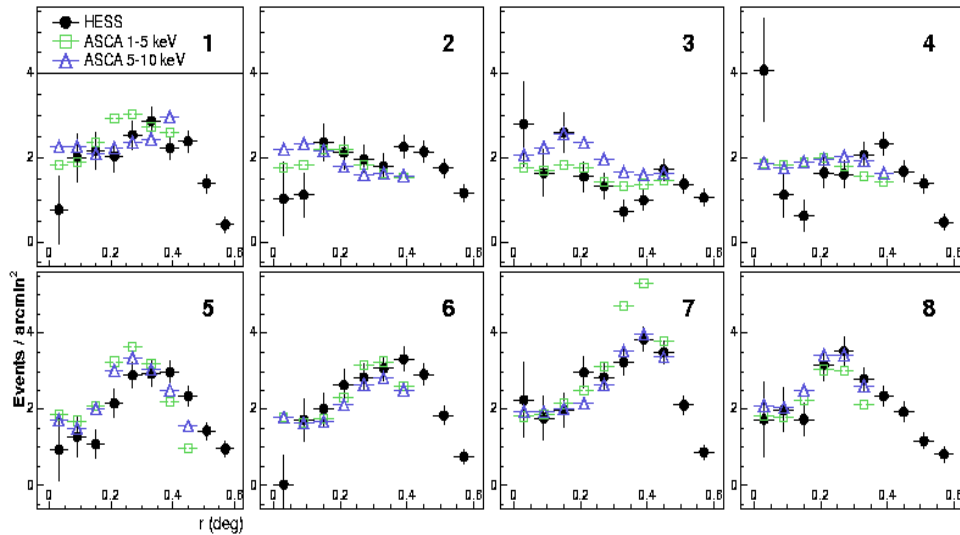


Figure 29: An overall 80% correlation is observed between TeV gamma rays (HESS) and X-rays (ASCA).

comparing their X-ray and γ -ray images and finding an excellent correlation between the two (Figure 29).

Modern X ray detectors, such as CHANDRA, have an excellent resolution and locate the SNR shock accurately (Figure 30).

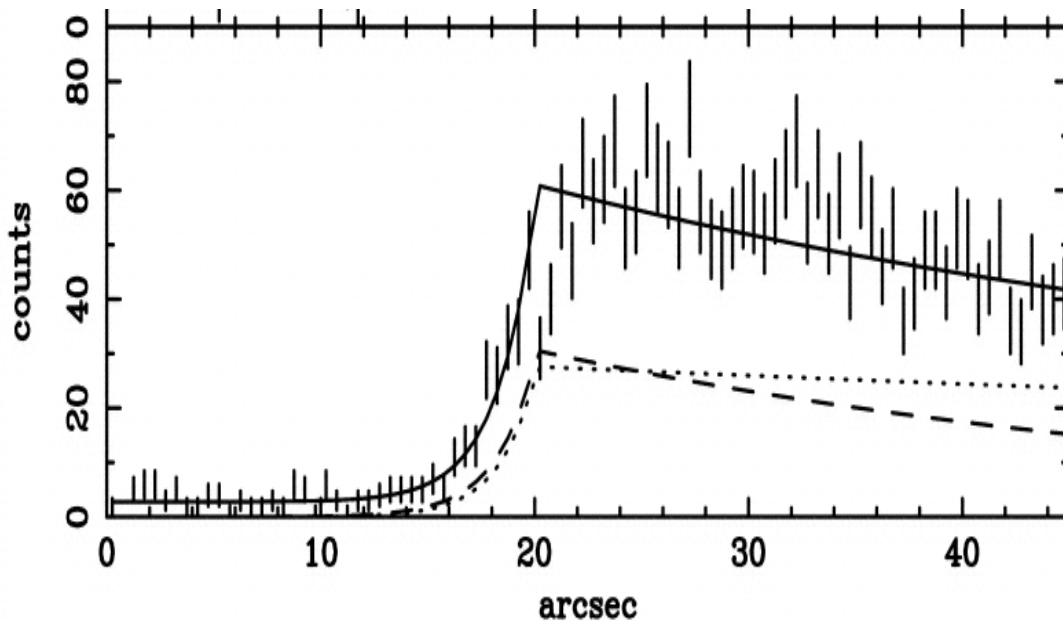


Figure 30: Precise definition of the shock from X-ray high resolution data.

Finally, at the higher energy end, Auger data show now a clear correlation of UHECR ($>6 \cdot 10^{19}$ eV) with nearby (<75 Mpc) galaxies (Figure 31). There is an even better correlation with nearby AGNs. The correlation disappears when including lower energy cosmic rays because they are bent by the galactic magnetic field. It also disappears when including farther away galaxies because of the GZK cut-off. Our environment (within the GZK horizon, below a radius of 100 Mpc or so) is extremely inhomogeneous (Figure 32).

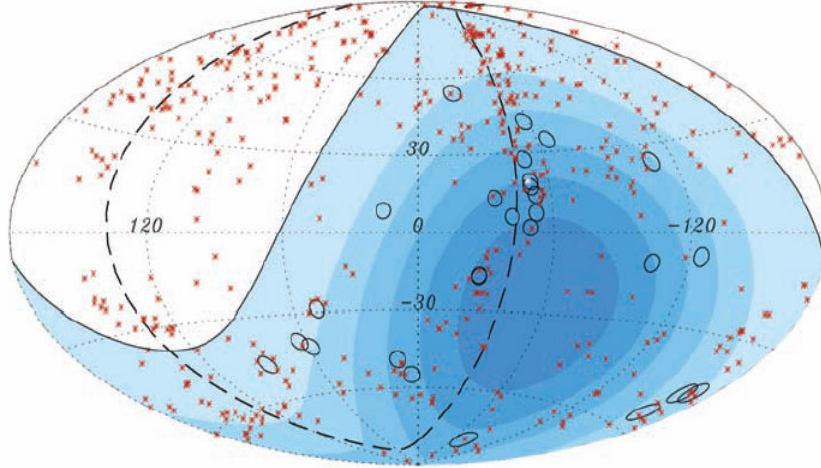


Figure 31: The highest energy UHECRs detected by the PAO (circles) are compared with AGNs within the GZK horizon (crosses). The dotted line is the supergalactic plane. The full line indicates the limit of acceptance.

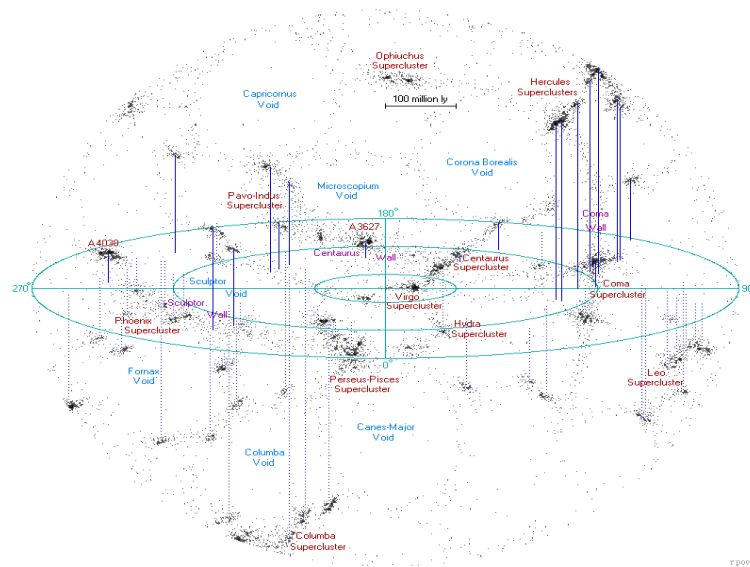


Figure 32: The structure of the Universe in our environment, within a radius of some 120 Mpc is very inhomogeneous with large voids, walls and filaments.

The correlation observed by the PAO is essentially a correlation with galaxies within this GZK horizon. This shows that the PAO is able to point to sources in the sky (typically within 1°), which was not a priori so obvious because of uncertainties in magnetic fields met by UHECR during their journey to the Earth (typically $3\mu\text{G}$ in the disk mean $6 \cdot 10^{17} \text{ eV}$).

A new page of astronomy has been opened as, until now, only photons could be used. It remains to be understood why such and such a galaxy, AGN or else, is a source while such and such another is not.

Not many celestial objects have a large enough value of the product magnetic field \times volume to be candidates for UHECR acceleration. The so-called Hillas plot (Figure 33) illustrates it clearly. Apart from magnetars which would suffer of excessive synchrotron losses, the only possible candidates are GRBs or active galaxies.

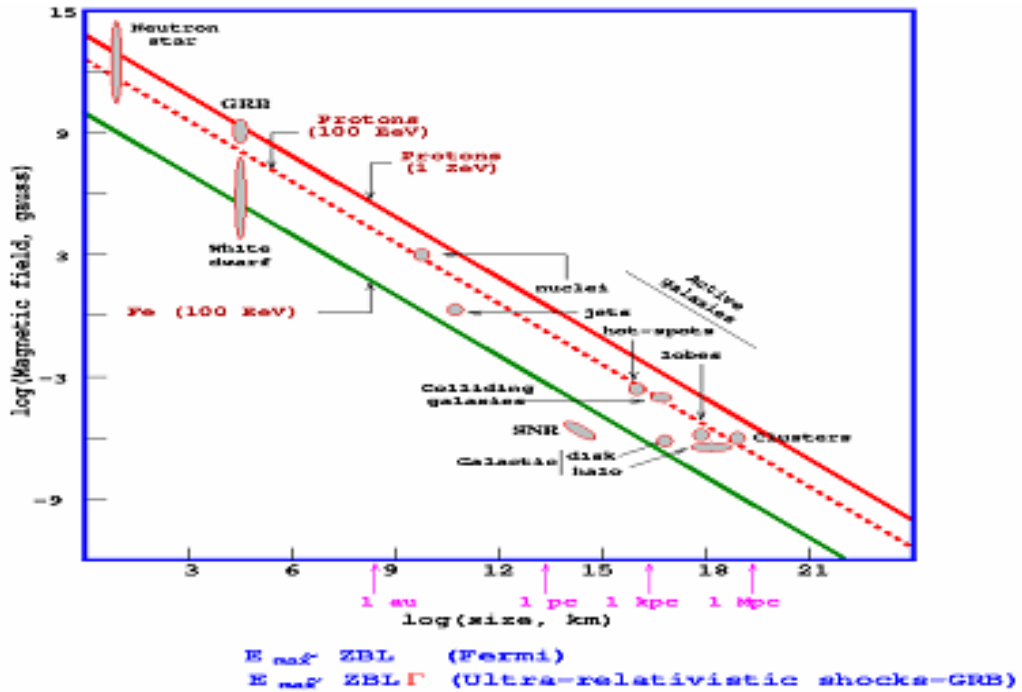


Figure 33: Hillas plot for 10^{21} eV protons (full red line), 10^{20} eV protons (dotted red line) and 10^{20} eV Fe nuclei (green line).

1.5 Acceleration in shocks

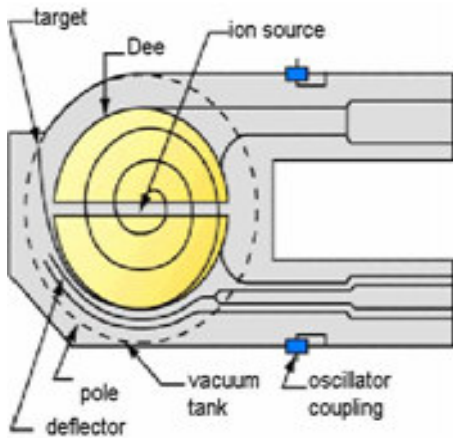


Figure 34: Schematic drawing of a cyclotron

The evidence for acceleration of galactic cosmic rays in the shell of young SNRs makes a process called diffusive shock acceleration (DSA) the most popular candidate for a universal acceleration mechanism. As in a cyclotron (Figure 34), the particle is accelerated locally on traversing the shock (equivalent of the gap between the dees) and is guided by magnetic fields on

either side in such a way as to come back to the shock (equivalent of the dipole guide field). However both the acceleration and guiding processes are very different from the cyclotron case. In particular guiding is provided by stochastic collisionless scattering on magnetic turbulences.

First order Fermi acceleration

Acceleration is best described in the shock frame where both upstream and downstream media move toward each other with large relative velocity β . Hence the energy $E+\Delta E$ of the cosmic ray (mass M) after having traversed the shock is given as a function of its energy E before having traversed the shock by a simple Lorentz transformation as $E+\Delta E = \gamma\beta E + \gamma p$ with $\gamma^2 = \gamma^2\beta^2 + 1$ and $E^2 = p^2 + M^2$. For $\beta \ll 1$, $\gamma \sim 1$ and for relativistic cosmic rays, $p = E$, giving $\Delta E = \beta E + O(\beta^2)$. Relation $\Delta E/E \sim \beta$ implies $E_n = E_0(1+\beta)^n$ after n shock traversals. One speaks of first order Fermi acceleration (first order in β). A stochastic succession of such processes nearly cancels: second order Fermi acceleration has negligible effects.

Interstellar medium and magnetic fields

To better understand the mechanism of DSA, it is essential to have a good picture of the interstellar medium (ISM) in which particles travel. The ISM is far from being a static medium but is continuously recycled through supernova explosions. It is made of three basic constituents: matter, magnetic fields and cosmic rays. In the Milky Way, matter amounts to 10-15% of the disk mass, half of it in clouds occupying 1-2% of the ISM volume, mostly very cold dark molecular and cold diffuse atomic. Elemental abundances are close to those in the solar system. About 0.5-1% in mass is in the form of dust. The main point in the present context is that ISM densities are so small that collisions with cosmic rays can be neglected: momenta (not energy !) change exclusively via the action of magnetic fields, one speaks of collisionless plasmas.

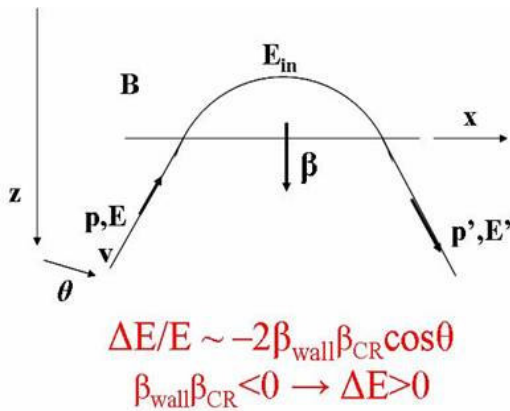


Figure 35 : Diffusion from a magnetic wall.

To understand how magnetic fields act as scattering centres, the (unrealistic) example of a magnetic wall (Figure 35) provides a good illustration (a magnetic bottle would be more realistic but less simple). Entering the wall, and then moving out, one has successively:

$$E_{\text{in}} = \gamma E - \gamma \beta p_z \text{ and } p_{z\text{in}} = -\gamma \beta E + \gamma p_z ;$$

$$E' = \gamma E_{\text{in}} - \gamma \beta p_{z\text{in}} \text{ (both } \beta \text{ and } p_{z\text{in}} \text{ change sign), namely } E' = \gamma^2(1+\beta^2)E - 2\gamma^2\beta p_z$$

which, for $\beta \ll 1$ ($\gamma=1$) becomes, using $p/E = \beta_{\text{CR}}$, $\Delta E/E \sim -2\beta_{\text{wall}}\beta_{\text{CR}}\cos\theta$. Of course the plasma which carries the magnetic field must recoil to balance the momentum reversal. It may look wrong that a magnetic field provides acceleration. But in the ISM frame the magnetic field is moving and it is of

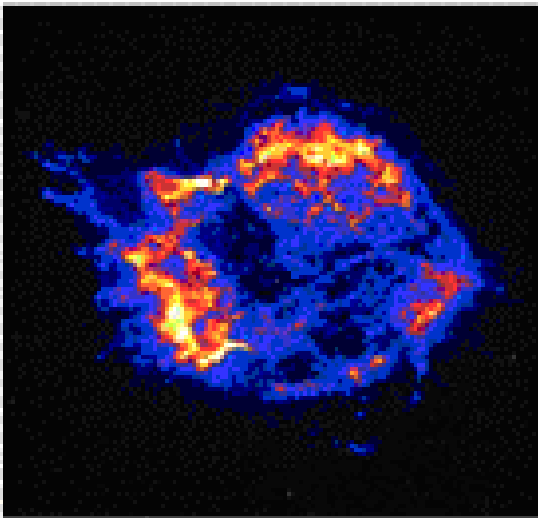
course the induced electric field that provides acceleration. In the magnetic volume, there is no electric field, but there is no acceleration either. Our knowledge of magnetic fields in the Universe, typically $3 \mu\text{G}$ in the disk of the Milky Way, comes from various observations: star light polarization due to spinning dust grains, Zeeman splitting of the 21cm H_I line and Faraday rotation of the plane of linear polarization of pulsar radio signals. The synchrotron radiation emitted by cosmic rays and detected in the all sky radio continuum also suggests a few μG scale.

Supernova remnants

It is useful to briefly recall the nature and structure of supernova remnants (Figure 36).

Type Ia supernovae are due to a white dwarf, member of a binary, accreting from its companion until it reaches Chandrasekhar mass (1.4 solar

Cassiopeia A (Chandra)



Crab Nebula (Chandra)

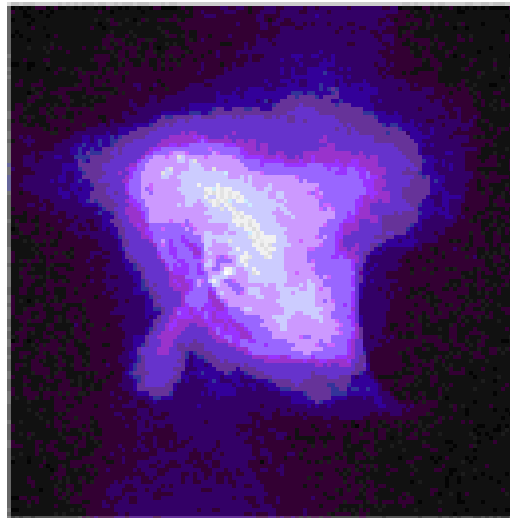
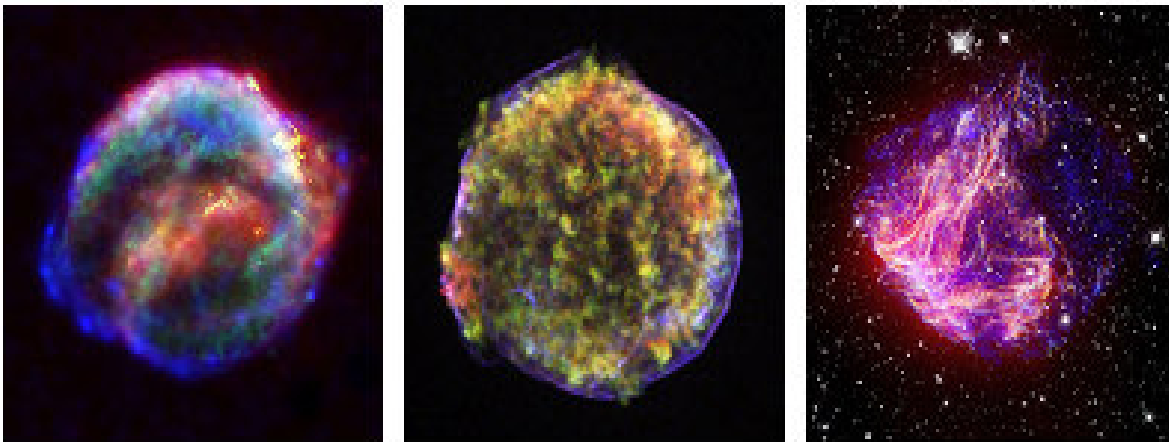


Figure 36: Cas A (left) is a young SN Ia, the Crab (right) a young SNI.

masses): the core is fully burned, the SNR shell is empty. Type II supernovae are due to a massive star collapsing into a neutron star that remains in the centre, possibly detected as a pulsar (Crab) the wind of which gives energy to the remnant (one speaks of a plerion). Modern X ray satellites provide very high resolution images of SNRs (Figure 37).



Kepler
SNR 1604

Tycho
SNR 1572

N 49

Figure 37: Three high resolution X-ray images (Chandra) of supernova remnants.

The explosion blast wave sweeps up the ISM in the forward shock (Figures 38 and 39). As mass is swept up, the forward shock decelerates and ejecta (having similar elemental abundances as the progenitor) are heated up by the reverse shock moving inwards. Nuclear reactions produce new heavy elements. Once enough mass has been swept up from the ISM (a few times the mass of the ejecta) the SNR enters the so-called Sedov phase. Thermal particles and magnetic fields are concentrated in the region of the shell while relativistic particles extend to much larger distances.

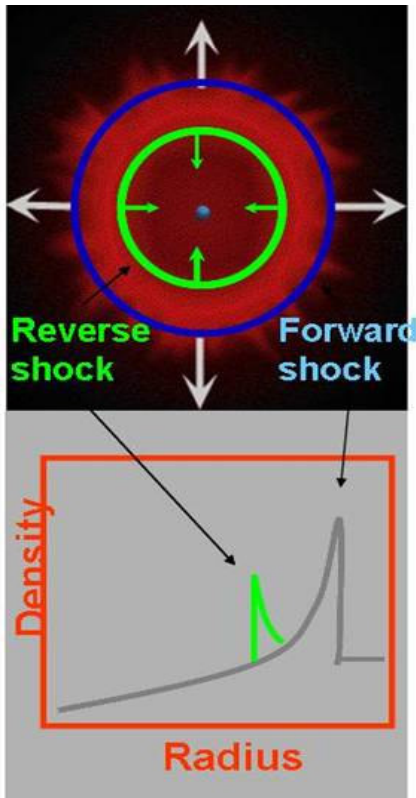


Figure 38: The shocks in a supernova explosion.

Synchrotron emission is confined to the magnetic field region. The shock structure depends on the age of the SNR: it is important to distinguish between young and old SNRs, the former being preferred acceleration sites for cosmic rays. In the case of plerions the situation is complicated by the presence of the pulsar wind (Figure 40) which sweeps up ejecta; the termination shock decelerates the flow and a so-called pulsar wind nebula (PWN) forms; while the SNR sweeps up ISM, the reverse shock heats ejecta and ultimately compresses the PWN.

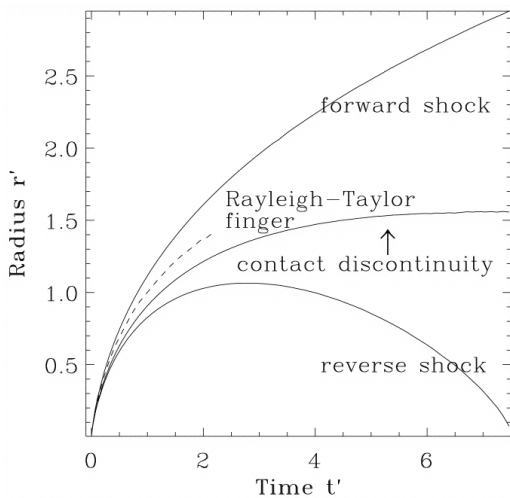


Figure 39: Time dependence of the shock progressions.

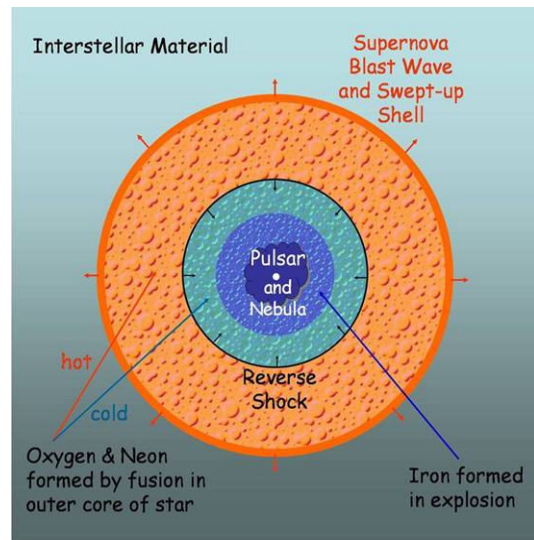


Figure 40: shock dynamics in a plerion.

Shock dynamics

In the case of a purely hydrodynamical shock (no magnetic field), the conservation of mass, energy and momentum on either side of the shock (expressed in the shock frame) defines the value of the compression ratio $r = \rho_2/\rho_1$ as $r = v_1/v_2 = (\gamma+1)/(\gamma-1) = 4$ for monoatomic gases (Figure 41).

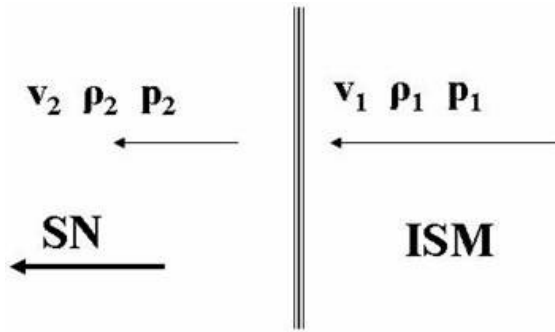


Figure 41: Shock dynamics, definition of variables.

Here ρ is the density, v the velocity and $\gamma = C_p/C_v = (3+2n)/(1+2n)$ (for gases having n atoms/molecule). The ratio of the shock velocity v to the sound velocity $v_s = \sqrt{\gamma p/\rho}$ is called the Mach number, $M = v/v_s$. In particular $v_1 - v_2 = 2v_1(1 - M_1^{-2})/(\gamma + 1) \rightarrow 2v_1/(\gamma + 1) = 3v_1/4$ for large Mach numbers and monoatomic gases: as the shock progresses into the unperturbed ISM the density increases suddenly by a

typical factor of 4.

On either side of the shock one sees the other medium approach at a velocity $v_1 - v_2$ and a relativistic cosmic ray crossing the shock at an angle θ gets always a first order Fermi acceleration $\Delta E/E \sim 2(v_1 - v_2) \cos\theta$. Taking $(v_1 - v_2) = 3v_1/4$ and $\cos\theta \sim 2/3$, one obtains an acceleration $\Delta E/E \sim V_{\text{shock}}/c$. It is important to be conscious that there is no collision in the process, but magnetic field volumes acting as scattering centres and aiming at each other on either side of the shock at relative velocity $v_1 - v_2$. The above calculation serves only as an illustration but is not really what we need: we need a model of these scattering centres and an understanding of how they evolve on crossing the shock. The conservation relations on either side of the shock

must of course include the magnetic pressure and energy density in addition to hydrodynamical quantities, but this is not enough: one needs to understand in detail the nature of the magnetic scattering centres and how they meet at the shock. This, however, is not well understood but only crudely modelled.

Energy spectrum

The rate of acceleration is given by the ratio of the relative energy gain when crossing the shock back and forth, $\Delta E/E \sim V_{\text{shock}}$, to the time Δt it takes. In the relativistic limit and in the approximation where the distribution of the scattering centres is irrelevant, the length of the trajectories scales with energy, $\Delta t \propto kE$. Once in region 1, the particle will always be caught by the shock, which is aiming toward it. However, once in region 2, it may escape the shock region for ever with a probability P_{esc} . In this region, the scattering centres move away from the shock at velocity $v_2 \sim \frac{1}{4}v_{\text{shock}}$ while the particle moves at light velocity at varying angles to the shock. Integrating over these angles, $P_{\text{esc}} = \beta_{\text{shock}}$. From the three basic relations, $\Delta E/E \sim \beta_{\text{shock}}$, $\Delta t \propto kE$ and $P_{\text{esc}} = \beta_{\text{shock}}$ one finds after n cycles, $E_n = E_0(1 + \beta_{\text{shock}})^n$. At each cycle only a fraction $(1 - P_{\text{esc}}) = (1 - \beta_{\text{shock}})$ survives. After n cycles $N = N_0(1 - \beta_{\text{shock}})^n$ particles survive having energy $E = E_0(1 + \beta_{\text{shock}})^n$. Hence $\ln(N/N_0)/\ln(E/E_0) = \ln(1 - \beta_{\text{shock}})/\ln(1 + \beta_{\text{shock}}) = -1$. Finally one gets $N = N_0(E/E_0)^{-1}$, namely $dN/dE \approx E^{-2}$. In general, for a compression ratio r , $dN/dE \approx E^{-\alpha}$ with $\alpha = (r+2)/(r-1)$. Diffusive shock acceleration results in a universal power law energy distribution.

Magnetic field amplification and turbulences

There exists copious evidence in favour of strong magnetic turbulences (Figure 42) and magnetic field amplification in the shock region of young SNRs. These play an essential role in the DSA process.

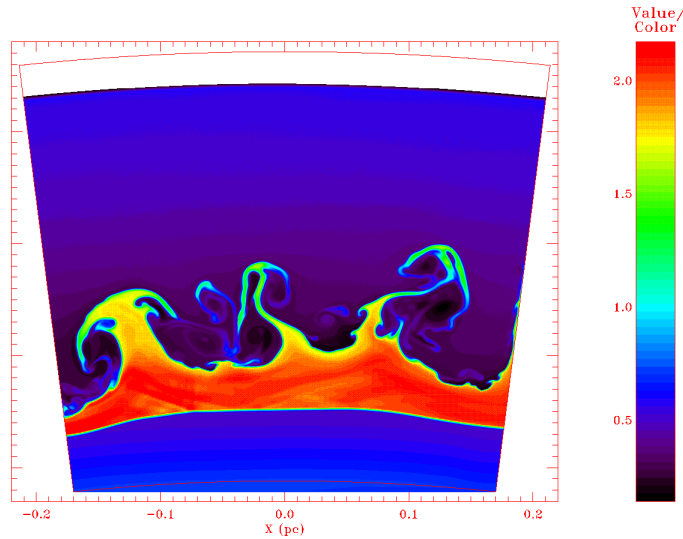


Figure 42: Turbulences simulated as density fluctuations in the region of the shock

Evidences for turbulences include important time variations of the non thermal X ray emission near the shock (Figure 43), observation of structures in the shell using high resolution X ray images: ripples (Figure 44) and filaments (Figure 45). Evidences for magnetic field amplification include a strong compression of the shock front (Figures 46 to 48), the comparison between non thermal radio and gamma rays emissions (the former are synchrotron radiations, sensitive to magnetic field, the latter are IC and neutral pion decays, insensitive to magnetic field). Field amplification factors reach two order of magnitudes in young SNRs. As cosmic rays and

the magnetized plasma carry similar energy densities, their mutual interactions have important effects.

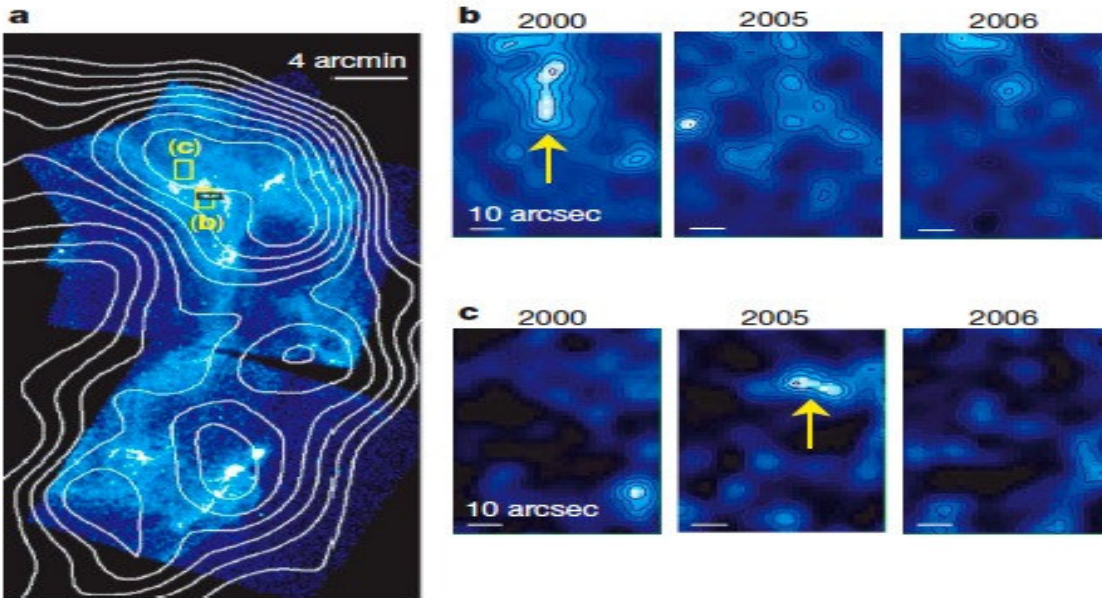


Figure 43: Strong variations have been noted in the intensity of X ray emissions over the years from the shell of RXJ1713.

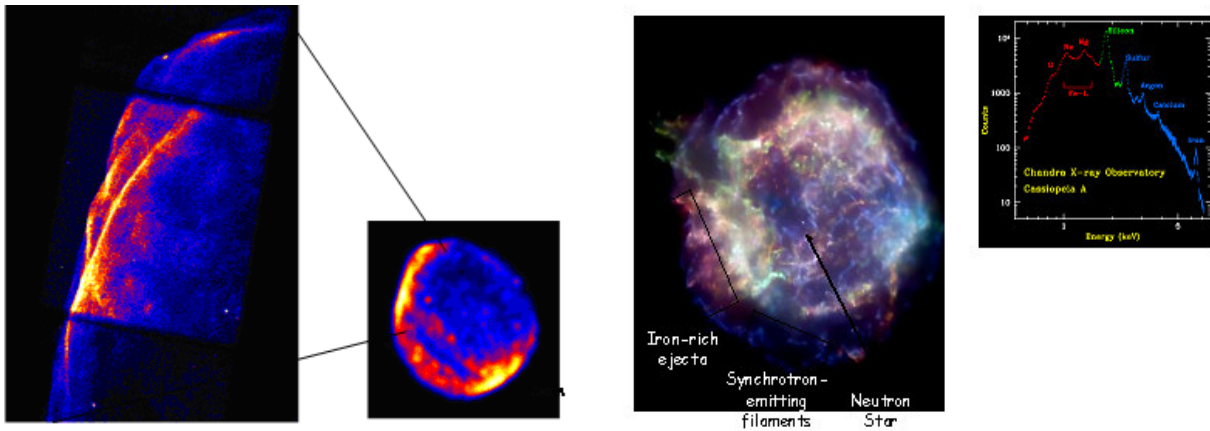


Figure 44: Ripples observed in the shock region of SN1006 .

Figure 45: Filaments observed in the shock region of Cas A.

Accelerated particles tend to stream ahead upstream, which causes the generation of streaming instabilities and makes the evolution non linear,

resulting in a strong amplification of the mean field. The structure of the shock is modified by cosmic ray retroaction. The higher field, in turn, depresses IC with respect to synchrotron emission, implying faster scattering and increased maximum momentum. Older remnants do not show such field amplification: the excitation of turbulences decreases with shock velocity, while damping (by non-linear wave interactions and ion-neutral collisions) does not. The energy contained in accelerated nuclei is about 100 times that in electrons.

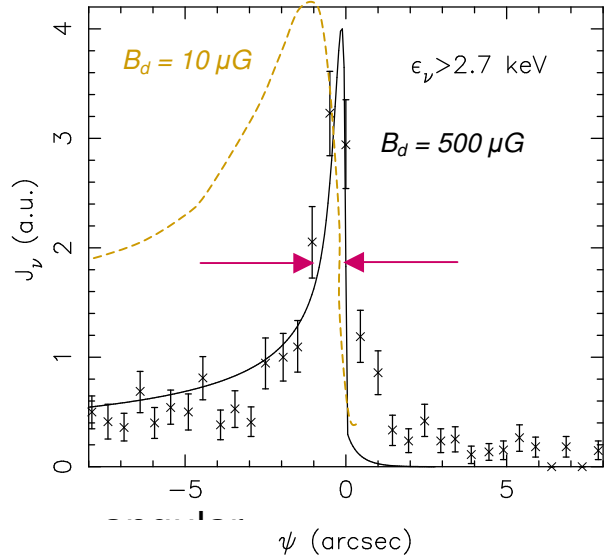


Figure 46: Compression of the shell of Cas A by a factor 50.

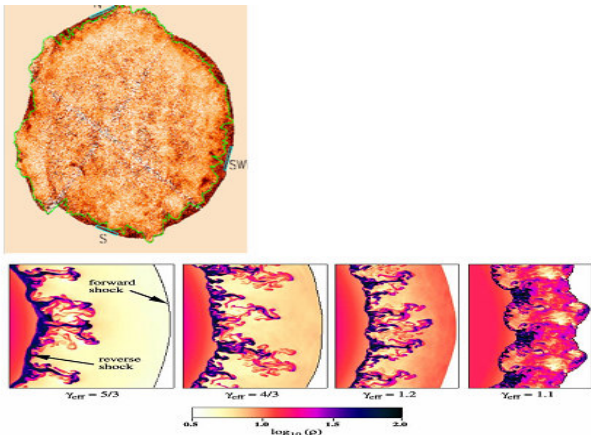


Figure 47: Tycho's discontinuity (green line) is very close to the front shock (top). Simulations show compressed shocks to accelerate cosmic rays efficiently (bottom).

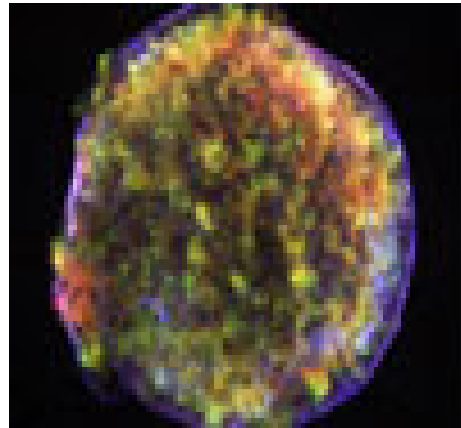


Figure 48: Compression of the shell of Tycho's SNR 1572.

1.6 Cosmic rays: a summary

Cosmic rays are accelerated atomic nuclei with elemental abundances as prevails in the Universe (apart from spallation reactions). They have a power law spectrum with index ~ 2.7 , cut-off at $\sim 10^{20}$ eV by interactions with the CMB; they contribute $\sim 1\text{eVcm}^{-3}$ to the energy density of the Universe, as much as visible light, CMB or magnetic fields; they play an important role in the ISM dynamics.

The Sun, wind and shocks, contributes to low energies. Most cosmic rays are of galactic origin and accelerated in the shells of young SNRs. Most UHECR have their sources in AGN rich regions. Recent progress in γ ray and UHECR astronomies have made cosmic ray physics a field of astrophysics in its own right

Spectacular progress in the understanding of the acceleration of galactic cosmic rays from SNR shocks suggests diffusive shock acceleration as a universal acceleration process. Magnetic turbulences and field amplification play an essential role. It seems possible to accommodate UHECRs in such a scenario as evidence in favour of sufficiently large scale shocks is now growing. Yet, many unknowns subsist on the details and the relevant collisionless plasma physics which governs the shock region is still not well understood. The focus and emphasis placed here on diffusive shock acceleration should not make one think that it must be the mechanism at play. It simply is the most likely scenario in the present state of knowledge. The years to come, in particular with the PAO identifying numerous UHECR sources, will teach us a lot.

2. Galaxy collisions

The survey of cosmic ray physics given in the preceding section suggested that it should be possible to accommodate UHECRs in a DSA scenario as evidence in favor of sufficiently large scale shocks is now growing. Such shocks may be found in colliding galaxies or merging galaxy clusters where active galaxies are numerous. The present section reviews recent knowledge in this field which has recently witnessed spectacular progress.

2.1 Generalities on galaxies

Galaxies are the fundamental building blocks of the universe They contain stars, in different stages of their evolution, gases, ionized and neutrals, and dust. One essentially distinguishes between two kinds of galaxies: spirals and ellipticals. However, smaller types, such as globular clusters (10^3 to 10^7 stars) and irregular galaxies (such as the Magellanic Clouds) are also found. The spirals contain a central hub and a thin disk while the ellipticals have a less well defined shape. Typical disk diameters and thicknesses are 10^5 ly and 10^3 ly respectively.

The very first galaxies formed only a few millions light years after the Big Bang. As we shall see, there are indications that they were smaller than the galaxies which formed later on but, as the Universe was much denser by then, they were often colliding or merging which resulted in the formation of larger galaxies.

Galaxies are grouped in clusters (and so called super clusters) of varying sizes. The Milky Way is part of the so called local cluster including Andromeda and the Magellanic clouds in its close by vicinity. Clusters may contain several tens to several thousands galaxies. At large scales the

Universe is seen to have a non homogeneous structure of so-called walls and filaments with gigantic voids in between.

Our galaxy is a typical spiral called the Milky Way and containing some 10^{11} stars. Most stars are similar to our Sun, burning hydrogen into helium; they are called Main Sequence stars. While the Universe is 14 billion years old, the Milky Way is about 10 billion years old, the Sun and the solar system around 5 billion years old. Our Sun will leave another 5 billion years before dying. Other stars are being born. They are formed from the condensation of hydrogen gas clouds. One can identify star forming regions from the large density of bright blue stars (OB associations).

The lifetime of a star depends on its mass, massive stars having a much shorter lifetime than light stars. Some, like is the case of our Sun, will end up as white dwarfs, compact and dense stars of the size of the Earth. Others, more massive than the Sun, will end up as neutron stars, which are much more compact and have a core of packed neutrons. They rotate very fast and often expel a jet of particles along their very large magnetic field: the resulting lighthouse effect makes pulsars. Their collapse is sudden and results in a very large release of energy, one speaks of a supernova. Their size is only a few kilometres.

When a star collapses, it expels in the interstellar matter a lot of material (in the form of planetary nebulae or supernova remnants) which will be later on recycled to produce new stars: like living bodies, galaxies keep recycling matter in successive generations of stars. Heavy elements are produced exclusively at the occasion of star collapses, elements produced in the interior of main sequence stars are essentially helium and more massive even-even nuclei (mostly carbon). We believe today that most, if not all, galaxies have a massive star, a black hole, in their centre. The Milky Way

has a central black hole of 3 million solar masses called Sagittarius A*. Some other galaxies have much more massive black holes in their centres, up to several tens of billions of solar masses. These are large objects (the size of a black hole is proportional to its mass, a radius of 3km per solar mass) and have a very bright accretion disk around them while, at the same time, ejecting two polar jets of electrons and possibly ions perpendicularly to the disk. They are called Active Galactic Nuclei, AGNs. As far as the arguments in the present work are concerned, we may ignore the peculiar properties of black holes as singularities of the gravity theory: they simply behave as very intense gravitational sources and what is going on around them, accretion disk, jets, etc..., is the simple result of this large gravity field.

2.2 Galaxy collisions: an introduction

It is now widely accepted that many galaxies (some astrophysicists estimate more than half) have been involved in one or more “collisions” with other galaxies, or even merged with galaxy clusters in their early life time. Such collisions were more common in the early much denser Universe when galaxies were much closer from each other. The word “collision” is put in quotes to emphasize the actual nature of the event. In effect, two galaxies that meet interact in the sense that they join into one with only a few stars actually bumping together in a destructive manner. The term “merge” is probably more descriptive of the process involved.

Kepler’s laws give a remarkably simple account of the movement of two point masses under gravity. Either they are bound and have elliptical trajectories, or they are unbound and stay unbound. Merging is simply not allowed in this simple case and one point mass cannot fall on the other and stay there! Reality is much more complex and merging occurs all the time. A

useful concept in this context is what is called tidal forces: when one of the point masses is replaced by an extended body, the part of that body which is closest from the point mass is more strongly attracted than the part which is farther away. A distortion of the extended body results in the form of a radial elongation. This is the origin of terrestrial tides. When the tidal forces are strong enough, they cause disruption of the extended body which may break in two or more parts, some of them being bound to the point mass and some other not. This concept of tidal forces is useful to visualize how a black hole can “swallow” matter in its accretion disk, or how a member of a binary, such as an X-binary or a future SN Ia, can “swallow” matter from its companion. In more complex cases, such as the condensation of a hydrogen cloud in the process of forming a (proto)galaxy, the concept of tidal forces is not of direct use: it only makes us aware of the complexity of the interaction. How an irregular cloud ends up in a set of perfectly spherical stars is not only a very complicated process but even a chaotic one: small changes in the initial conditions may result in drastic differences in the final result.

Such is the case of colliding galaxies. When two galaxies happen to have proper movements (one says peculiar movements, usually with velocities at the scale of some 10^{-4} c) such that the distance of closest approach between their trajectories (meaning the trajectories which their centres of mass would follow if the galaxies were not interacting with each other) is of the same scale as their sizes, the two galaxies will collide, meaning that while approaching each other they will suffer very important distortions. The probability for two stars to collide in the normal sense of the word is essentially negligible as stars are so far apart from each other with respect to their own sizes. However, in the process, the average gravity field in the collision volume will be strongly increased and this is likely to have

important consequences. Indeed, we know how important are the effects of density increases such as those induced by the density waves making the arms of spiral galaxies or by the shock waves of supernova explosions, or simply by the presence of a strong gravity field such as is the case in the centre of the Milky Way in the environment of Sgr A*, a three million solar masses black hole. They trigger the birth of new stars from the hydrogen clouds present in the region, with many blue bright stars appearing, typically of the O and B types. The heavier of these have a short life time and explode in supernovae before the other stars have a chance to drift away, inducing a kind of chain reaction with new stars being born and new supernovae exploding until enough of the matter in the environment has been blasted away to form what is called a bubble or super bubble. Such activity results in an increase of the density of stellar black holes, SNRs, X binaries, etc... and if it takes place in the central region of the galaxy its central black hole will accrete more matter and grow in mass and in size. Therefore one expects that these very same phenomena will take places in the event of galaxy collisions in the regions where the resulting density increases are strongest.

Depending on their sizes and shapes, and on their relative movement before collision, colliding galaxies can be expected to display very different behaviours. The usual end product of the merging of two spiral galaxies is an elliptical galaxy and many elliptical galaxies are thought to have formed this way. In some conditions, however, collisions can also give rise to spiral structures. The diversity of the collision patterns is illustrated in the following examples. The Cart Wheel galaxy (Figure 49) is the result of a collision between a smaller galaxy having passed through a larger one; both

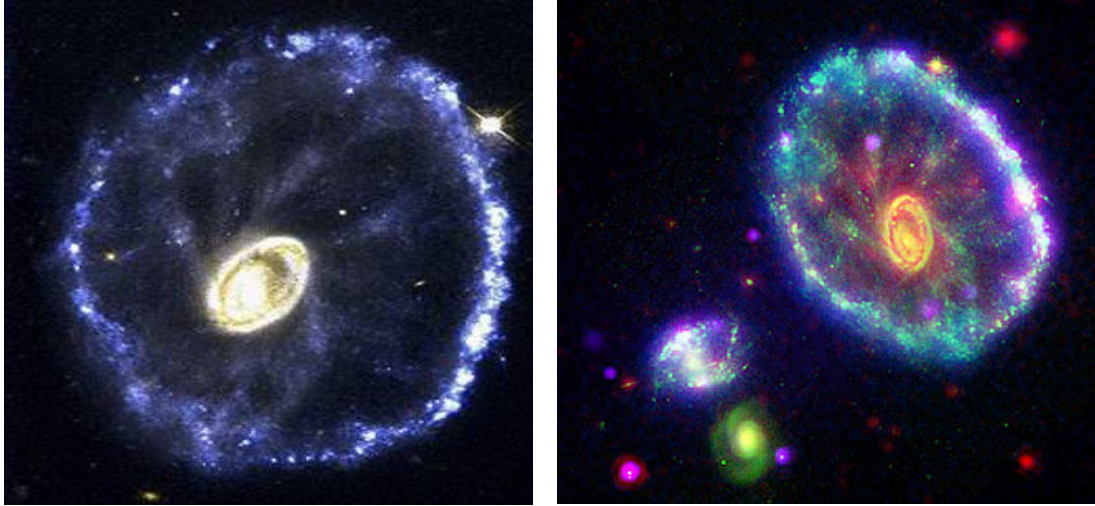


Figure 49: The Cart Wheel galaxy, collisions between two galaxies.

galaxies are still visible and a gigantic ring of new born stars was formed in the induced density shock wave.

The Antennae galaxy (Figure 50), some 20 Mpc away from us, shows two galaxies in the process of colliding. Here again a high density star formation region on a path joining the two galaxies is visible.

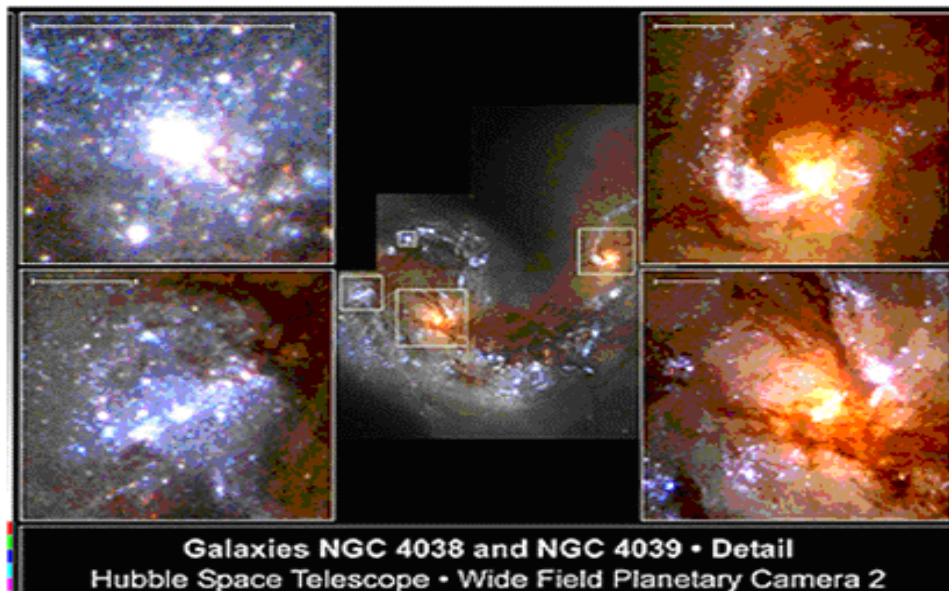
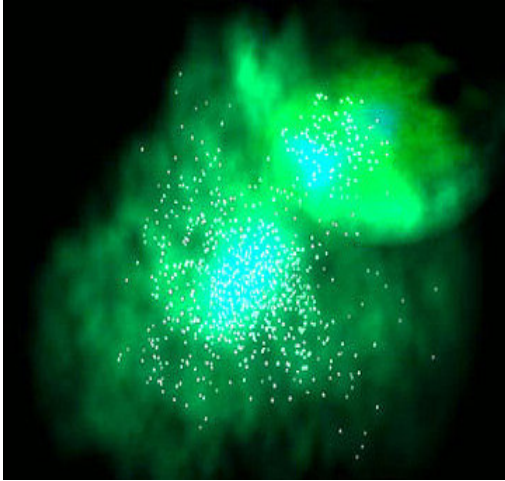


Figure 50: The Antennae Galaxy, collision between two galaxies, shows very dense star forming regions.



Figures 51: X ray image of colliding clusters in Abell 754.



Figures 52: X ray images of colliding galaxies in NGC 1700.

The X ray images (Figures 51 and 52) of colliding clusters in Abell 754 and of colliding galaxies in NGC 1700 reveal copious amounts of energy being radiated. In particular, in the case of NGC 1700, a collision between a spiral and an elliptical 50 Mpc away from us, CHANDRA has detected a huge release of X-rays stemming from the elliptical galaxy.

In general observation at different wave lengths, in particular radio, infrared and X-rays, are essential to understand what is going on. Figures 53 and 54 display other examples of colliding galaxies at different stages of their evolution. There exist also numerous examples of more than two galaxies colliding, such as shown in Figures 55 and 56.

These examples illustrate the complexity and the diversity of the phenomenon and witness the intense stellar activity which such collisions do trigger. It is not surprising, under such conditions, to find that galaxy collisions host very large shocks which can be excellent candidates for accelerating UHECRs (Figure 57).

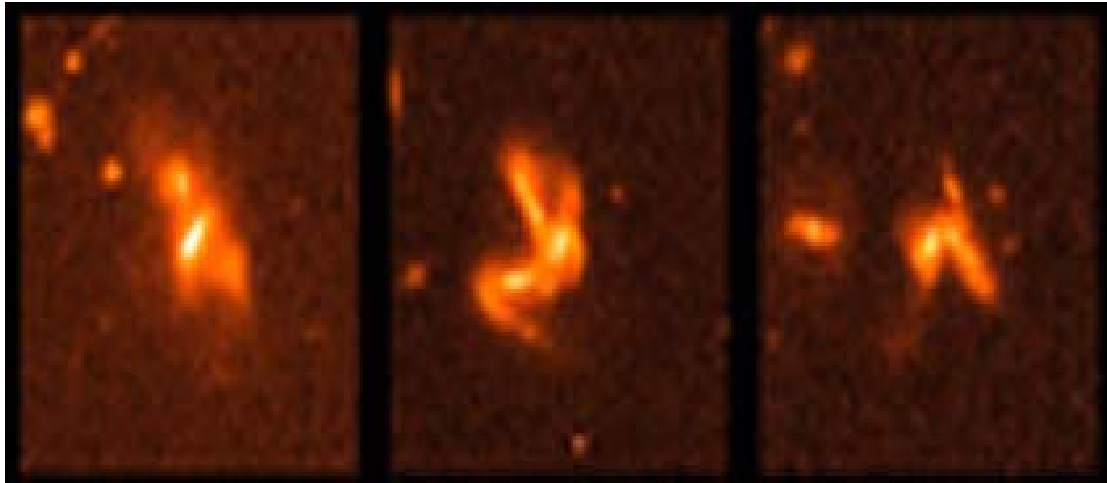


Figure 53: HST images of colliding galaxies in the infrared.

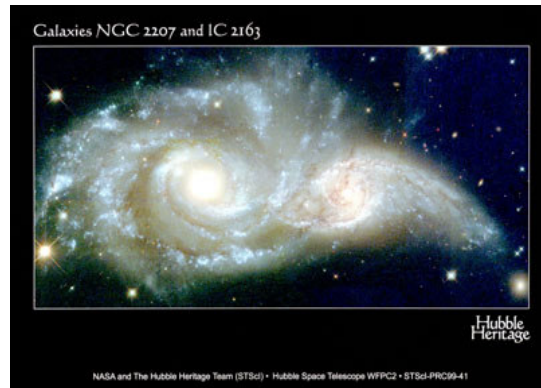
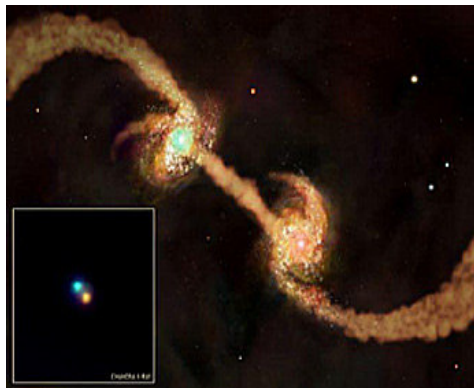


Figure 54: HST images of colliding galaxies.



Figure 55: Stephan's quintet.



Figure 56: Multiple galaxy collisions.

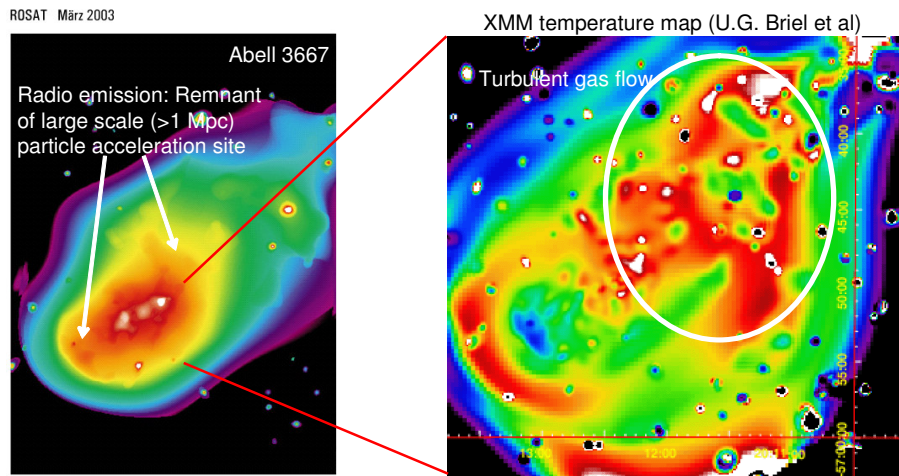


Figure 57: Evidence for turbulent gas flow and large shocks in Abell 3667 (X ray image from XMM).

2.3 Active galactic nuclei (AGN): an introduction

We already mentioned black holes in several occasions earlier and we noted that as far as the present work was concerned one could think of black holes as simply very massive objects with a radius proportional to their mass, 3 km per solar mass. For most practical purposes, the main difference between a black hole and a neutron star is that the mass of the former is unlimited, while that of the latter cannot increase beyond 2 to 5 solar masses (above this limit it becomes a black hole!). Indeed black holes span a gigantic mass range, from a few to billions of solar masses.

One usually distinguishes between stellar black holes and galactic black holes. Stellar black holes have been produced in a supernova explosion as the end product of the life of a massive star. There are many of these in the Milky Way and similar galaxies. On average, in the Milky Way, there are two supernova explosions per century. Their masses remain at the stellar scale, typically ten solar masses. Galactic black holes are located at the centre of galaxies and their masses may reach billions of solar masses.

The most massive of these trigger an intense activity in the host galaxy that becomes the seat of extremely violent events.

We suspect today that there is a galactic black hole in the centre of each galaxy, at least of each spiral galaxy. The reason for this suspicion is the recent evidence collected in favor of the presence of black holes in the centre of several nearby galaxies, in particular Andromeda, and, more importantly, in the centre of our own galaxy, the Milky Way. Until recently, the observation of the galactic centre was prevented by the presence of a large cloud of dust that hides it from our view. This cloud, however, is transparent to radio waves and the presence of a strong radio-emitter in the centre of our galaxy has been known for now thirty years. It is called Sgr A* (Sgr stands for Sagittarius, the constellation where the galactic centre is located). Infrared observation allows for resolving many of the brightest stars in the region of the galactic centre where the density of stars is enormous, one million times higher than around our Sun. Recently one of these, that has a very elongated orbit around the galactic centre, could be followed accurately while passing near focus and revealed the presence of a 3 million solar mass black hole in the region of Sgr A*. Moreover, X ray observation in this region of many X-ray binaries suggests the concentration around Sgr A* of a swarm of ten thousand or so stellar black holes. These and other observations suggest that stellar black holes produced in a supernova explosion migrate to the centre of the galaxy and end up feeding the galactic black hole around which they first get gravitationally trapped. The Milky Way being 10 billion years old, it would take an average absorption rate of no more than 10^{-3} stellar black holes per year for SgrA* to have reached its current mass.

Another important difference between a black hole and a neutron star is the inability of the former to be traversed by magnetic field lines as a neutron star does (one says that black holes have no hair), the field is expelled from the horizon a bit like in the Meissner effect of superconductivity. However, in practical cases, an accreting black hole spins rapidly and traps gigantic magnetic fields in its accreting disk, itself anchored to the equator of the horizon of the spinning (Kerr) black hole. But, contrary to pulsars, the magnetic dipole moment of accreting black holes is always aligned along the axis of rotation. The gyroscopic effect (conservation of angular momentum) implies a very high stability of the direction of this axis, as testified by the fact that the jets of quasars show no measurable curvature, implying no significant movement over the quasar lifetime.

Compact objects, with a strong gravity field near their surface, such as white dwarfs, neutron stars and black holes, can accrete matter from a companion or from the matter in their environment. Accretion in a disk around a rotating object is observed at very different scales. The mechanism of trapping of matter in a gravitational field and of the possible formation of an accretion disk is complex. Accretion disks around compact

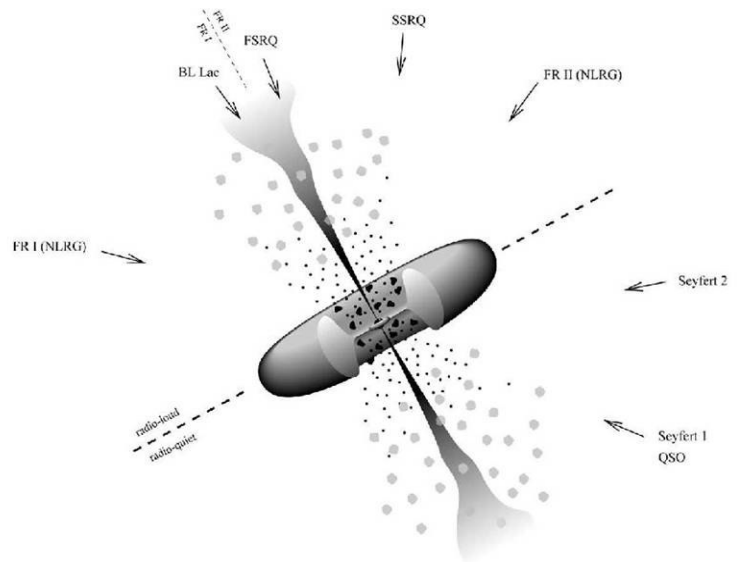


Figure 58: Schematic structure of an AGN

objects such as neutron stars and black holes play a particularly important role. Two mechanisms are at play in the formation of an accretion disk, the effect of tidal forces, and the multiple collisions that take place in the disk. Accretion from a black hole can become very spectacular in the case of super massive black holes surrounded by a dense medium. One believes today that many of the most spectacular events in the visible universe are indeed the results of such events. The general picture (Figure 58) is that of a black hole in the centre of a galaxy, spiral or elliptical. The black hole is very massive, say 10^8 solar masses (typical galaxies have masses of the order of 10^{11} solar masses). The gas and the stars in its neighbourhood “fall” on it. The gas condenses in a disk around the black hole and ionizes, spinning faster and faster as it comes closer to it, exactly as predicted and very well reproduced by simulations. While speeding up the gas gets hot and radiates at X-ray frequencies. The (inward) flux of accreted matter is limited by the (outward) resistance offered by the photons radiated in the process. This kind of self-regulation implies an upper limit for the luminosity L of an accreting black hole of a given mass M . Its value, $L(\text{erg/s}) \sim 10^{38} M(\text{solar masses})$, is called the Eddington limit. From the observed luminosity of the brightest quasars one infers this way enormous mass values for the central accreting black hole, up to 10 billion solar masses! Around the accreting disk one finds a torus of dust that is opaque to visible light. The strong magnetic field anchored in the spinning plasma of the disk creates two jets propelling electrons and ions at very high energies along the disk axis. Synchrotron radiation in the jets gives a strong photon emission over a very broad frequency range. At variance with the pulsar case, the magnetic field and rotation axes are exactly the same. Moreover, the rotating black hole behaves as a gyroscope and the direction of the jets remains absolutely

invariant as testified by their absence of curvature (despite their very long extensions). Such systems are generically called Active Galactic Nuclei (AGN) and cover many different observed objects such as quasars, Seyfert galaxies, BL Lac, blazars, etc...

Quasars (Figure 59), standing for quasi-stellar radio sources, were discovered as

being intense radio-sources (the radio-lobes at the ends of the jets) coinciding with very distant, compact (no apparent diameter) and bright star-like optical objects (the accretion disc). Rapid (on the scale of several days) and erratic variations of the optical luminosities are observed, confirming that the star-like object is very compact. Quasars are observed to emit over a broad range of photon frequencies. In most cases two radio lobes can be resolved on either side of the nucleus at typical distances of 100 kpc, sometimes linked to it by a narrow radio jet (Figure 60).

Radio galaxies are sometimes classified into two different families, FRI and FR II, depending on the angle between the jets and the line of sight. Many elliptical galaxies have been observed to behave similarly to quasars while not being such strong radio emitters as quasars are.

Seyfert galaxies are understood today as being quasars having a nucleus luminosity not quite as strong as quasars have: the accretion disc does not hide (blind) the surrounding galaxy (one speaks of type 1 Seyfert

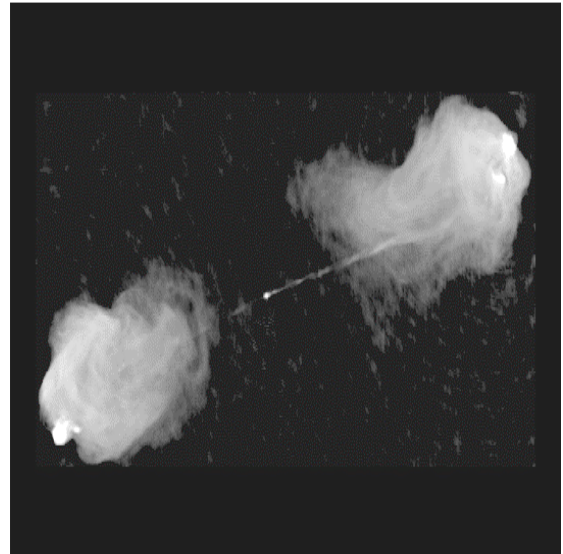


Figure 59 : A radio (VLA) image of radio galaxy Cygnus A, showing the accretion disk (the bright spot in the middle), the jets and the radio lobes.

galaxies). Galaxies having similar spectral features but showing no central nucleus (type 2 Seyfert galaxies) are of the same kind but the nucleus is now hidden by the dust torus (as evidenced in the infrared). Depending whether a Seyfert galaxy is seen from a region close to its axis or close to its equatorial plane, it will appear as a type 1 or type 2 respectively.

BL Lacertae (or Lacertides, or BL Lac), first thought to be variable

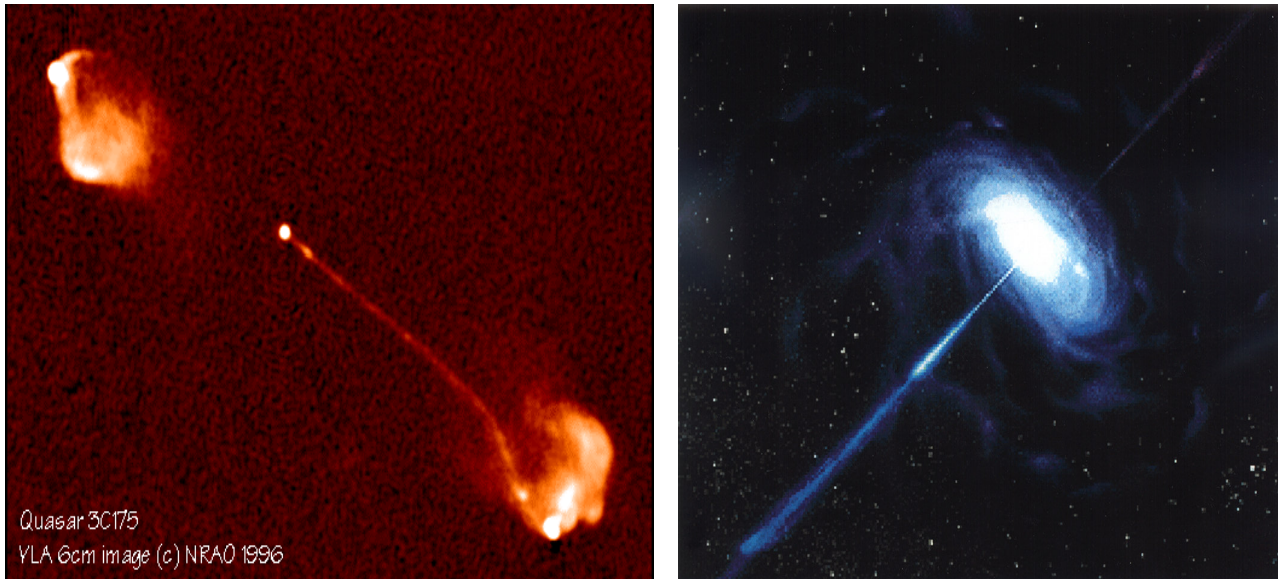


Figure 60: Two radio images of quasars showing clear jets and lobes.

stars, were later found to be a compact galactic nucleus associated with an intense radio-source. A remarkable feature is that the radio emission comes from two regions that are observed to recess from each other at very high velocities. Such configurations correspond to cases where one of the jets is approximately pointing toward the earth and the other away from it. For such AGN configurations one sometimes observes the emission of very high energy gamma rays: one then talks of blazars; they exhibit rapid flux

variability in essentially all measured frequency bands, from radio to gamma rays.

2.4 Centaurus A: presentation

Centaurus A, itself much larger than the Milky Way, is a known hot spot in both X-rays and radio waves. It is only 10 million light years away from us and is the closest active galaxy. Also known as NGC 5128, it is a peculiar galaxy in the constellation of Centaurus of which it is the strongest radio source. It is part of a group of 25 galaxies extending over about 25° in the austral sky. In addition to NGC 5128, major members of the group are NGC 4945 and NGC 5236. NGC 5128 is the only massive elliptical in the group. The members have an average projected radial distance to the centre of mass of 0.72 Mpc. The group is probably still collapsing. Assuming a distance of 3.4 Mpc, the group mass estimate becomes $5-17 \cdot 10^{12}$ solar masses. It is quite remarkable that the other two major members, NGC 4945 and NGC 5236, exhibit signs of unusually vigorous star formation, while NGC 4945 also has a nuclear out flow. In addition, the dwarf galaxies in the group have relatively high central surface brightness and exhibit clear star formation activity. NGC 5128 is itself a strong X-ray source.

With magnitude 7, NGC 5128 is the fifth brightest galaxy in the sky, immediately after the Local Group members M 31, M 33, LMC and SMC. The light distribution closely follows the $(1 - r/r_0)^{1/4}$ de Vaucouleurs law characteristic of elliptical galaxies. However, the appearance of NGC 5128 departs strikingly from that of a normal elliptical galaxy because of its broad and patchy equatorial dark band (Figure 61). The dark band is associated with young stellar objects. It is in fact a thin, strongly warped disk embedded in the host galaxy that creates the superficial appearance of a broad band.

Kinematically, the galaxy and the dark band represent different entities. The elliptical system and the globular clusters associated with it have low rotational velocities, whereas the dust disk exhibits much higher rotational velocities. These features are taken as evidence for NGC 5128 to be in fact a pair of colliding galaxies made of a small spiral embedded into a larger elliptical.

With its 90 kly diameter, NGC 5128 is the largest X-ray source yet discovered in the Universe. The emissions come from a vast spinning cloud of hydrogen gas excited to temperatures in excess of 8 million degrees and associated with the interaction between the spiral and elliptical galaxies.

2.5 Centaurus A: two galaxies

A closer look at NGC 5128 illustrates the evidence for it being in fact a pair of colliding galaxies. Figure 61 shows Centaurus A as seen optically through a ground-based telescope, the AAO (Anglo Australian Observatory) and through the Hubble Space Telescope (HST) Wide Field Camera in what is called the DSS (Digitized Sky Survey). An elongated disc, marked by dark dust, is spread across a large white glow that is identified as an elliptical galaxy. Other close-up views of the inner region have been obtained by the Very Large Telescope, a ground-based telescope in Chile (Figure 62). Comparing the DSS and AAO images one notes that the DSS image is over-exposed in the central region. However, this brings out fainter emission features elsewhere in the field of view, and allows a better view of dust (seen in silhouette) in the outer regions. The bright stellar content of the galaxy resembles an elliptical galaxy containing several billions of stars. An obscuring band of dust, however, is more often associated with spiral galaxies.

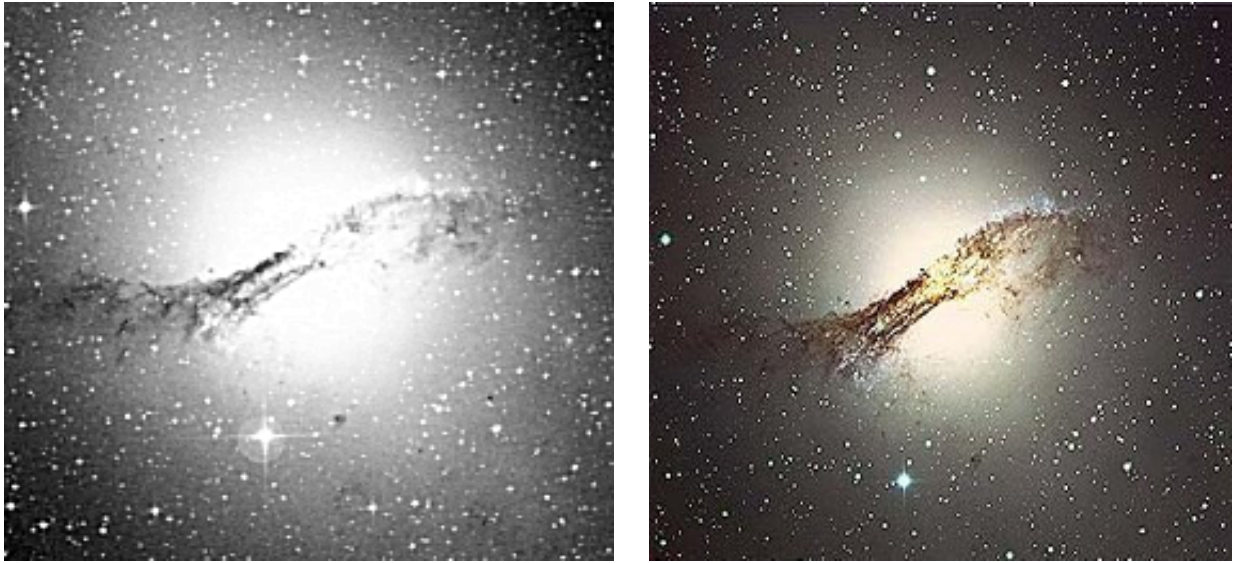


Figure 61: Optical images of Cen A from space (left, HST/DSS) and ground (right, AAO).



Centaurus A
(MPG/ESO 2.2-m + WFI)

ESO PR Photo 14a/03 (10 June 2003)

© European Southern Observatory



Figure 62: Optical images of Cen A from the ESO telescopes in La Silla (Chile). The recent image on the right uses the high resolution detector FORS2 on the VLT.

Furthermore, looking closely at the northern edge of the dust lane, about 5 arcmin to the north-west (upper right of Figure 62) of the image centre, one sees a region where young and hot blue stars have recently formed, a feature usually seen along the dusty arms of spiral galaxies. The dust band encircling Centaurus A is heavily distorted, suggesting that something strange has taken place here.

Infrared photons can penetrate the dust to reveal a hot, turbulent mass of stars, dust and gas from the spiral galaxy falling into the core of the elliptical one. Infrared images from ISOCAM are shown in Figure 63. Some of the dust inside Centaurus A maps out what appears to be a barred spiral galaxy, which has recently merged with its giant elliptical host and is feeding gas into the host's central hole, clearly resolved, to produce bi-polar jets that are bright in radio and X-ray wavelengths.

Figure 64 shows a short-exposure mosaic of images taken at three near-infrared wavelengths on ground by 2MASS (2 Microns All Sky Survey). The most noticeable feature is the bright central condensation of stellar emission. The intervening dust lane is much less conspicuous than at visible wave lengths. This is due to the fact that near-infrared light can pierce through all but extremely dense concentration of dust.

Figures 65 and 66 show images taken at longer infrared wavelengths. In this regime, most of the infra red emission is produced by dust grains. The mid-infrared picture (Figures 65) was obtained with a camera aboard the Spitzer Space Telescope at wavelengths of 3.6 to 8 microns. This image clearly reveals the flattened inner disk of the spiral galaxy that once rammed into the elliptical galaxy.

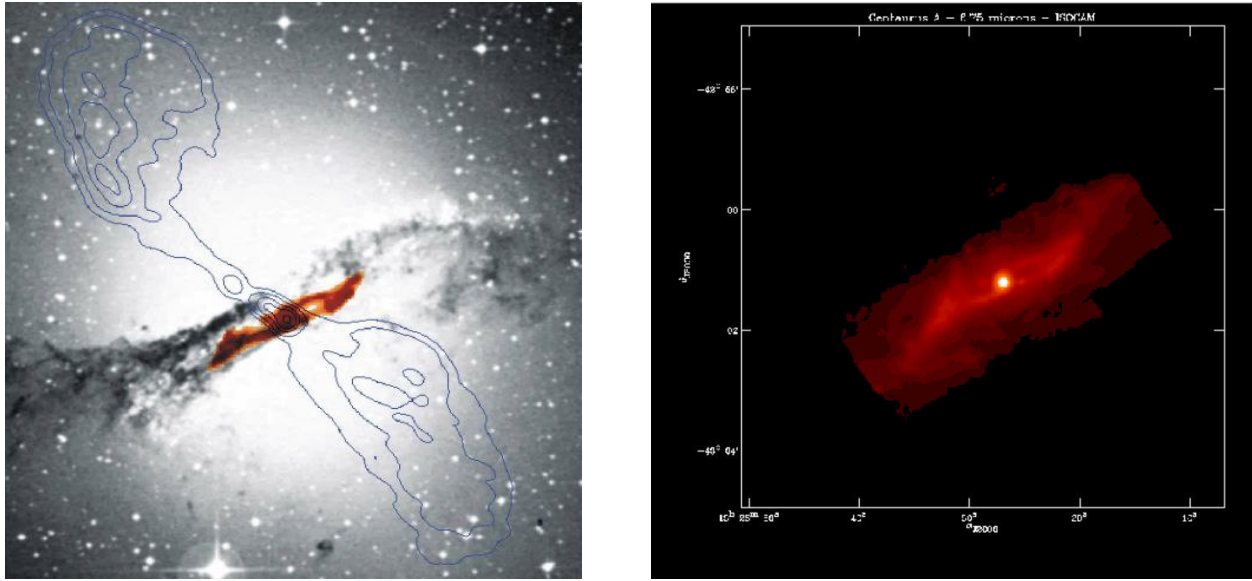


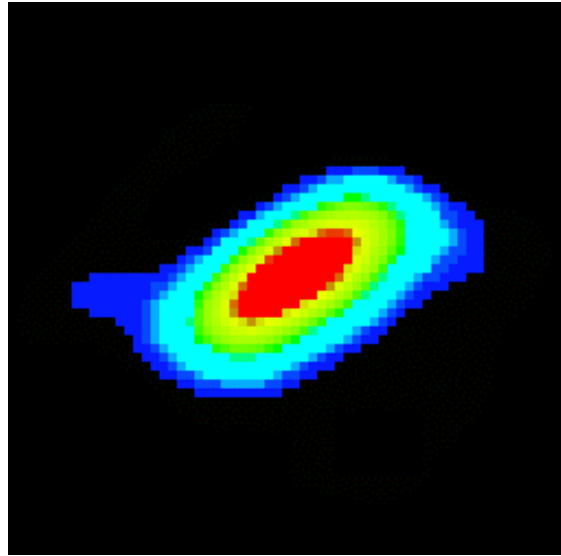
Figure 63: Two infrared images of Cen A taken from the ISO satellite. The image on the left (in red) is superimposed on an optical image in black and white and on radio contours showing the jets and lobes. The image on the right is a recent high resolution ISOCAM image resolving the accretion disk.



Figure 64: Near infrared images of Cen A taken from ground by 2MASS.



Figures 65: Mid infrared image of Cen A taken by Spitzer.



Figures 66: Far infrared image of Cen A taken by IRAS.

The low-resolution far-infrared photograph (Figure 66, IRAS) is able to distinguish only a central peak of long-wavelength emission, stretched along the same orientation as the dust disk seen in the Spitzer image.

The recent images of ISOCAM (Figure 63) and Spitzer (Figure 65) show the warped and twisted disk of the spiral galaxy devoured by Centaurus A having dust shaped like a parallelogram around 1,000 ly wide. The parallelogram lies along the active galaxy's central band of dust and stars visible in more familiar optical images. Astronomers believe that the striking geometric shape represents an approximately edge-on view of the infalling spiral galaxy's disk in the process of being twisted and warped by the interaction. Ultimately, debris from the spiral galaxy should provide fuel for the super massive black hole lurking at the centre of Centaurus A. Detection of the spiral's dust in a bi-symmetric structure provides strong evidence of its

position deep inside the giant elliptical host while the vast amounts of radio, visual, and X-ray emissions are a result of the energy released by this continuing galactic merger.

In summary, visible light images of Centaurus A resemble an elliptical galaxy. Its prominent dust band, however, is not a feature normally associated with ellipticals which are generally quite dust poor and populated with old stars. Recent observations in infrared suggest that the galaxy is actually a giant elliptical that is in the process of devouring a smaller dusty, barred spiral galaxy similar in size to prominent nearby spiral M 33. The collision would have taken place hundreds of millions of years ago. There are arguments for the giant elliptical's gravity helping the barred spiral to maintain its shape. In turn, material funnelled along the spiral's bar fuels the central black hole which powers the elliptical's radio lobes.

2.6 Centaurus A: the central AGN

Evidence for Centaurus A being an active galaxy rests mostly on radio and X-ray observations. Centaurus A is a bright radio source which shines in the radio sky as illustrated in the 400 MHz radio map shown in Figure 67. At such frequencies, radio waves are generated by high energy electrons spiralling along magnetic fields (synchrotron radiation). The map shows the galactic plane running horizontally through the centre, but no stars are visible. Instead, many of the bright sources near the plane are distant pulsars, star forming regions and supernova remnants. Centaurus A is clearly visible above the plane to the right of centre, while the LMC shines below and right.

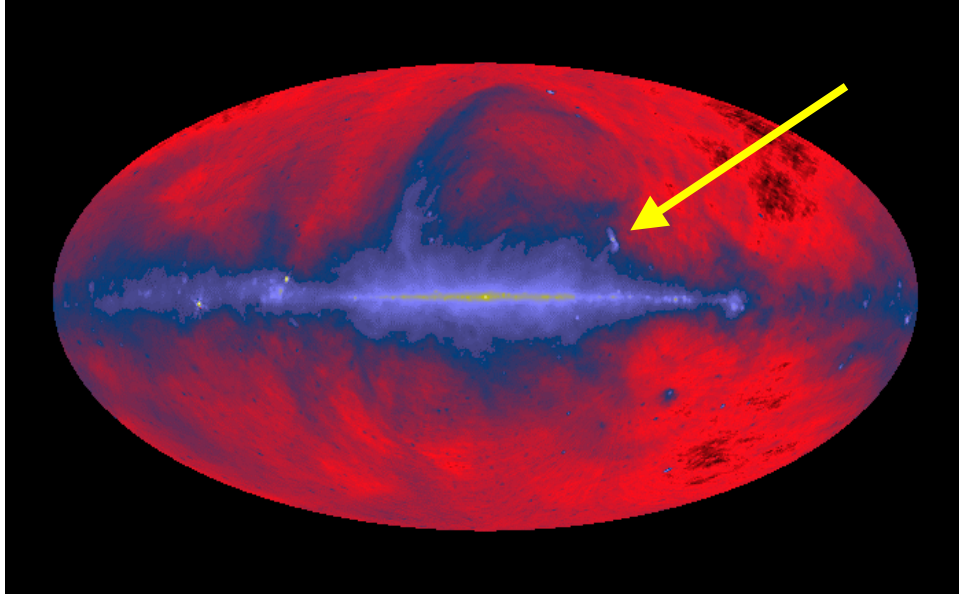


Figure 67: 400 kHz radio map of the sky in galactic coordinates.
The arrow points to Cen A.



Figure 68: Radio image of Cen A (VLA, 6cm).

Figure 68 shows a radio image obtained at a wavelength of 6 cm at the Very Large Array, an array of radio telescopes in New Mexico, and it shows a remarkable feature unlike any seen in the previous photographs (apart from the radio lobes shown in Figure 63): A pair of narrow jets appears to be shooting out of Centaurus A, with the radio emission becoming more diffuse at greater distances from the galaxy centre. The radio jets consist of plasma, a high-temperature stream of matter in which atoms have been ionized and molecules have been split apart. These jets are nearly perpendicular to the dust disk, as seen when the radio emission contours are overlaid on a visible-light photograph (Figure 63).

Figures 69 and 70 show X-ray views of Centaurus A obtained by Chandra (CXO), one of NASA's "Great Observatories". The most dominant feature is an X-ray jet extending some 15 000 light years towards the northeast (upper left). A less prominent jet extends towards the south-west. The apparent brightness difference between the jets is probably due to the viewing geometry. One believes that the first jet is moving towards us, while the second is moving away. These observations provide additional evidence that an invisible and super massive black hole is nestled in the centre of Centaurus A.

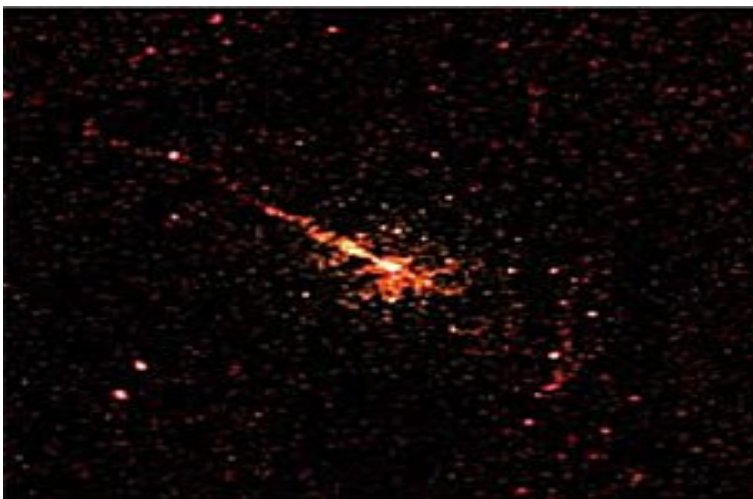


Figure 69: X ray image of Cen A obtained by Chandra.



Figure 70: A very recent (January 2008) CHANDRA image of Cen A.

The image in Figure 70 represents the equivalent of more than seven days of continuous observations by CHANDRA. A prominent X-ray jet extending for 13,000 ly points to the upper left of the image, with a shorter counter-jet aimed in the opposite direction. Turbulent knot-like features in the jets show where the acceleration of electrons to high energies is currently occurring, and provides important clues to understanding the process that accelerates them. The inner part of the X-ray jet close to the black hole is dominated by these knots of X-ray emission, which probably come from shock waves caused by the jet. Farther from the black hole there is more diffuse X-ray emission in the jet.

Hundreds of point-like sources are also seen in the Chandra image. Many of these are X-ray binaries that contain a stellar-mass black hole or neutron star and a companion star in orbit around one another. These isolated X-ray sources clustered around the galaxy centre are reminiscent of the similar observations made around Sgr A*. The image shows two particularly bright X-ray binaries. These sources may contain stellar mass black holes that are unusually massive. In this image, low-energy X-rays are coloured red, intermediate-energy X-rays are green, and the highest-energy X-rays detected by Chandra are blue. The dark green and blue bands running almost perpendicular to the jet are dust lanes that absorb X-rays. They were created when Centaurus A merged with the other galaxy some 100 million years ago.

Another observation that reveals the activity of Centaurus A is the gamma-ray image taken by the now extinct Compton Gamma-Ray Observatory above 100 keV where Centaurus A is clearly visible. However, the low-resolution of the gamma ray detectors prevents a study of the finer details, such as jets, to be made. Moreover, at higher energies, no significant emission has been observed: both Cangaroo and HESS see no significant gamma ray flux above 1TeV which is surprising if Cen A is a UHECR acceleration site as suggested by the PAO data.

Finally, Figure 71 shows an image of Centaurus A taken by GALEX in ultra violet. The dust lane absorbs the ultraviolet light from the stars in the galaxy. However, where the jets seen by Chandra interact with clouds of hydrogen gas located some 50 kly away from the galaxy centre, several regions of ultraviolet (UV) emission can be seen in the north-east (upper left) just beyond the X-ray emission. This UV light may be from young stars

formed in a burst of recent star formation triggered by the compression of the gas clouds by the X-ray jet.



Figure 71: Ultraviolet image of Cen A by GALEX.

2.7 Centaurus A: other features

Figure 72 shows a composite X-ray (blue), radio (pink and green), and optical (orange and yellow) image of Centaurus A. A broad band of dust and cold gas is bisected at an angle by opposing jets of high-energy particles blasting away from the super massive black hole in the nucleus.

Two large arcs of X-ray emitting hot gas were discovered in the outskirts of the galaxy on a plane perpendicular to the jets. The arcs of several million degree gas appear to be part of a projected ring 25,000 light years in diameter. The size and location of the ring indicate that it may have been produced in a titanic explosion some ten million years ago.



Figure 72 Composite image of the central region of Cen A: X ray (blue), radio 21 cm and continuum (pink and green), optical (orange and yellow)

Such an explosion would have produced the high-energy jets, and a galaxy-sized shock wave moving outward at speeds of several parts in thousand of the light velocity. The age of 10 million years for the outburst is consistent with optical and infrared observations that indicate that the rate of star formation in the galaxy increased dramatically at about that time.

As was mentioned earlier, evidence that Centaurus A's activity is the result of a merger with a smaller, gas-rich galaxy is given by the bright young blue stars (Figure 62) seen along the edges of the dust band that elliptical galaxies normally do not have enough gas to form. The galaxy is also surrounded by faint shells of gas and dust along which an arc of blue stars, a few thousands light years large, can be seen (Figure 73). Although faint shells around galaxies are not unusual, they are strong evidence of previous galaxy mergers, which leave ripples like on the surface of a pond.

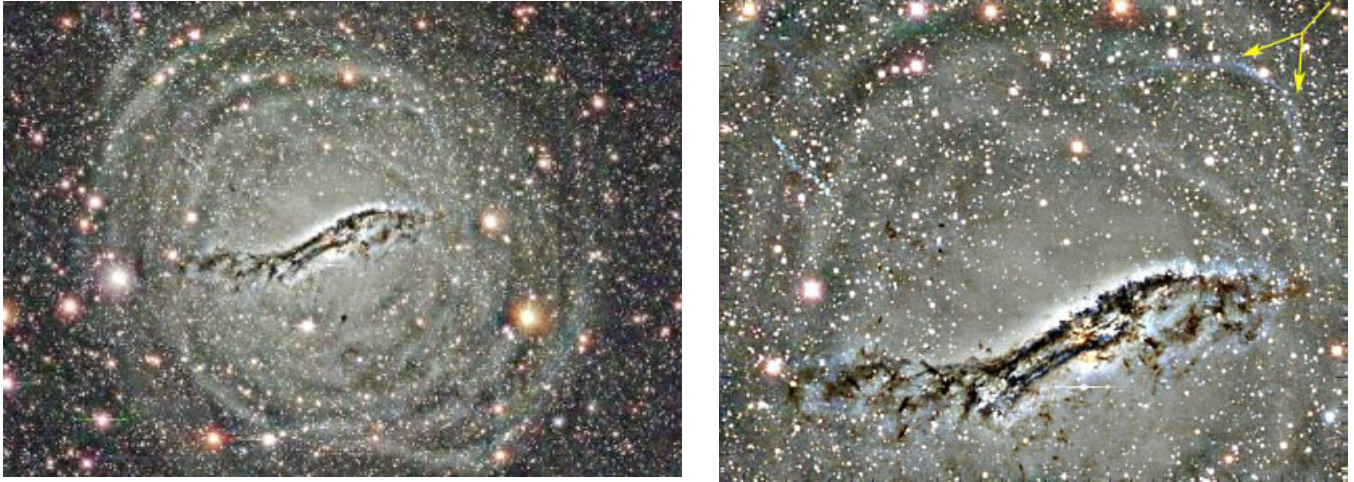


Figure 73: Concentric shells (left) and a blue arc of young blue stars (right, yellow arrows) are visible around the galaxy

An unexpected attribute of these shells is the abundance of gas, which may have become separated from the smaller galaxy during the collision. The tidal forces of the larger, host elliptical galaxy caused a burst of star formation within the in falling galaxy, and these young stars were then spread along the remnant of the incoming orbit.

In recent years, intermediate-age and young stellar populations in the halo of Centaurus A have been detected at the European Southern Observatory (ESO). The youngest stars appear to be aligned with the powerful jet produced by the massive black hole at the galaxy's centre. In 2003, thousands of very luminous and red, long-term pulsating variable stars that are similar to Mira Ceti, have been discovered, thus confirming the presence of a population of intermediate-age stars in Centaurus A's halo.

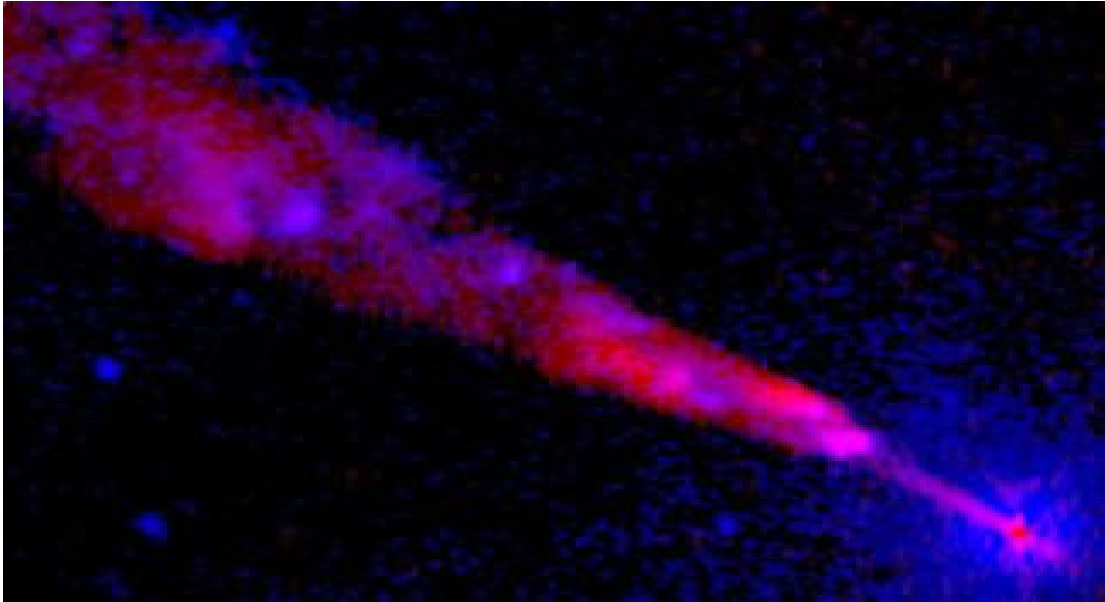


Figure 74: High resolution composite image of one of the Cen A jet.

Figure 74 shows a composite image of Chandra X-ray (blue) and VLA radio (red) observations showing the inner 4,000 light years of the north-east magnetized jet of Centaurus A. Purple regions are bright in both radio and X-ray. The jet originates from the vicinity of the super massive black hole at the centre of the galaxy (lower right hand corner of the image). The radio observations, taken between 1991 and 2002, showed that the inner portion of the jet is moving away from the centre of the galaxy at speeds of about half a percent of the speed of light. Most of the X-rays from the jet are produced farther out where the jet stalls as it plows through the gas in the galaxy. The collision of the jet with the galactic gas generates a powerful shock wave that produces the extremely high-energy electrons responsible for the X-rays.

Because Centaurus A jet is relatively nearby at a distance of 11 million light years, this image offers one of the most detailed looks yet at the interaction of a jet with gas in its galaxy.

The dark band crossing the elliptical galaxy, associated with the spiral, is known to consist of a metal-rich population of stars, nebulae and dust clouds. Metallicities are close to those in the solar neighbourhood; the disk is at position angle $122^\circ \pm 4^\circ$ and star formation is rampant. The present burst of star formation (Figures 62 and 73) apparently started 50 million years ago and created at least a hundred HII regions embedded in the disk. Star formation may occur there in OB associations at rates ten times higher than in the Milky Way. As defined by its OB stars and HII regions, the disk extends out to a radius of 4 kpc.

The disk is in rapid rotation. The HII regions are distributed throughout the warped disk and embedded in diffuse ionized gas. The HI observations show the atomic hydrogen to follow the dust lane, including the warp. Measured values of the HI mass range between 300 and 800 million solar masses. Total molecular hydrogen masses are probably about 400 million solar masses. The total gaseous mass of the disk, including helium, is thus of the order of 10^9 solar masses, only about 2% of the dynamical mass contained in the elliptical component within the radius of the disk.

The central region of the galaxy, within a few hundred parsec from the nucleus, is very complex. The nucleus itself, hidden behind thick dust clouds, is visible at infrared millimetre and centimetre wavelengths (Figures 63 and 65) and again at high energies, but generally requires very high resolutions to separate it from its surroundings. Infrared and millimetre observations on CO emission have established the presence of a compact circumnuclear disk with an estimated gas mass of 10 million solar masses.

Its outer radius is 110-280 pc and it contains a central region of radius 40 pc, devoid of CO. Such a 100 pc-scale disk appears to be a common feature of active galaxies. The total dynamical mass within the disk area is estimated at about 10^9 solar masses, i.e. a hundred times higher than the molecular gas mass. Its major axis is at position angle 140° - 145° , some 20° away from that of the dust band, but perpendicular to the position angle of the jets .

The enormous mass within the central region cannot be caused by normal stars, as it would then be much more luminous, but by a super massive black hole having most likely a mass of some 200 million solar masses. Indeed, recent infrared spectroscopy measurements of the stellar kinematics using the spectral region around the CO band give masses ranging between 150 and 240 million solar masses depending on inclination with typical uncertainties of 30 million solar masses.

The galactic foreground confusion caused by the low galactic latitude of NGC 5128 for a long time impeded attempts to identify its globular clusters. However, after the first identifications were finally made the number of confirmed globular clusters rose steadily to 87 in 1992 while the total population is estimated at 1550 ± 350 . Globular cluster studies have been used primarily to extract information on the galaxy's metallicity and dynamics, as well as its distance.

In terms of both numbers and metallicities, the globular cluster system of NGC 5128 appears to be normal for large elliptical galaxies or indeed for spheroidal components of galaxies in general. The clusters in NGC 5128 seem to have somewhat greater metallicities than their Milky Way counterparts and seem to form two families. This is of great interest in view of the proposed merger-nature of the galaxy, particularly as a bimodal

metallicity distribution with metal-rich clusters more concentrated than metal-poor clusters is known to be a natural consequence of galaxy mergers.

A survey of [OIII] emission from planetary nebulae in NGC 5128, extending over 20 kpc along the major axis and fully covering the central 10 kpc, yielded 785 detections. A colour-magnitude diagram of 10000 red giant branch (RGB) stars in the halo of NGC 5128 was constructed from HST/WFPC2 images, the first time that individual stars were resolved in a spheroid system beyond the Local Group. About 200 stars were found to be brighter than the tip of the RGB; their luminosity functions suggest the presence of an intermediate-age population of about 5 Gy, but making up at most 10 % of the total halo stellar population.

The galaxy was the host of the type Ia supernova 1986g which reached a maximum of absolute magnitude $M_B = -19.6 \pm 0.5$.

Summary and perspectives

The relative proximity of Centaurus A, together with its particularly interesting structure, has made it one of the most studied and most instructive celestial objects. It illustrates the importance and power of multiwavelength observations.

Infrared astronomy has shown in a spectacular way the dual structure of Cen A with a barred spiral seen nearly edge-on in its very centre. Indirect evidence is given by the different rotation velocities and metallicities of the two components.

Radio and X ray astronomies have demonstrated the AGN nature of Cen A with a super massive black hole in its centre. The jets and radio lobes have been observed with remarkable resolution, providing evidence for

turbulences associated with the acceleration of electrons and related emission of synchrotron radiation.

As in the case of the other galactic black hole in our neighbourhood, Sgr A*, other phenomena have been observed, which reveal the presence of the black hole: large density of X ray binaries, presence of a circumnuclear ring, etc. The mass of the super massive black hole has been measured between 150 and 240 million solar masses by stellar kinematics in infrared spectroscopy, again reminiscent of the Sgr A* case.

Signs of a gigantic explosion having occurred some ten million years ago have been detected in the farther environment of Cen A in the form of X ray arcs and of density waves enhancing star formation.

Other observations, such as of globular clusters and variable stars, have confirmed the dual and AGN nature of Cen A.

These observations and their interpretation suggest that the many other sites of galaxy collisions which have been identified in the sky at larger distances from us are likely to be the seat of similar phenomena. In particular, they are excellent candidates for hosting large shocks at galaxy scales where UHECR could be accelerated via diffusive shock acceleration. However, the current non-observation of TeV gamma rays from Cen A may shed some doubt on this interpretation, even though Cen A is known as a gamma emitter in the 100 keV region. In the coming years, the accumulation of statistics in the identification of UHECR sources by the Pierre Auger Observatory will be essential in clarifying such issues and will undoubtedly shed much new light on this fascinating chapter of physics.

Bibliography

Basic information on astrophysics and cosmology is from lectures by Pr Pierre Darriulat at the National University of Sciences and at various schools in Quy Nhon, Hanoi and Kathmandu.

The dissertation of my elder colleague Kim Thi Phuong on Sgr A*, also written under guidance of the VATLY team, has been of much help.

Most of the information used in the present dissertation has been obtained from various web sites where proper credits can be found:

Introduction

nedwww.ipac.caltech.edu/level5/March01/Israel/Israel_contents.html
iop.org/EJ/abstract/1538-3881/130/2/406
coolcosmos.ipac.caltech.edu/cosmic_classroom/multiwavelength_astronomy/multiwavelength_museum/cenA.html

Colliding galaxies

rst.gsfc.nasa.gov/Sect20/A4.html
rst.gsfc.nasa.gov/Front/tofc.html
rst.gsfc.nasa.gov/Sect20/A6.html
csep10.phys.utk.edu/astr162/lect/galaxies/colliding.html
curious.astro.cornell.edu/question.php?number=351
noao.edu/outreach/current/collide_hilite.html

AGNs

en.wikipedia.org/wiki/Active_galactic_nucleus
imagine.gsfc.nasa.gov/docs/science/know_11/active_galaxies
pnas.org/cgi/content/full/96/9/4749
astro.uchicago.edu/home/web/everett/agnOverview/agnOverview.html

Cen A

seds.org/messier/xtra/ngc/n5128.html
solstation.com/x-objects/cent-a.htm
solstation.com/x-objects/cent2a.jpg (fig 62)
solstation.com/x-objects/cent2spi.jpg (fig 63)
solstation.com/x-objects/cent2gal.jpg (fig 65)
solstation.com/x-objects/cent2arc.jpg (fig 72)

chandra.harvard.edu/photo/2002/0157/0157_composite.jpg (fig72)
solstation.com/x-objects/cent2sh.jpg (fig 73)
jhu.edu/news_info/news/home02/oct02/galaxy.html (fig 73)
solstation.com/x-objects/cent2jets.jpg (fig 70)
solstation.com/x-objects/cent2jet.jpg (fig 74)
mpe.mpg.de/~hcs/Cen-A
mpe.mpg.de/~hcs/Cen-A/Pictures/cent-a-chandra-20080109.jpg (fig 70)
mpe.mpg.de/~hcs/Cen-A/Pictures/Cen-A-Legende.jpg (fig 62)
mpe.mpg.de/~hcs/Cen-A/Pictures/galaxy-radio408mhz-2.gif (fig 67)
mpe.mpg.de/~hcs/Cen-A/Pictures/cent-a-radio6cm.jpg (fig 68)
eso.org/outreach/press-rel/pr-2003/pr-13-03.html
astr.ua.edu/gifimages/cena.html
natiomaster.com/encyclopedia/Centaurus-A-Galaxy
J.D. Silge, K. Gebhardt, M. Bergmann and D. Richstone, *Astr. J.* 130
(2005)406.